Title: Initiation of DNA replication requires actin dynamics and formin activity

Authors:

Nikolaos Parisis[1,2,5,8,9], Liliana Krasinska[1,2,9], Bethany Harker[1,2,3], Serge Urbach[2,4], Michel Rossignol[5], Alain Camasses[1, 2], James Dewar[6], Nathalie Morin[2,7], and Daniel Fisher[1,2,*]

Affiliations:

[1] Montpellier Institute of Molecular Genetics (IGMM), CNRS UMR 5535, 34293 Montpellier, France.

[2] University of Montpellier, Faculty of Sciences, 34090 Montpellier, France.

[3] Present address: Wellcome Trust Centre for Cell Biology, University of Edinburgh, EH9 3QR Edinburgh, UK.

[4] Functional Proteomics Platform (FPP), Institute of Functional Genomics (IGF), CNRS UMR 5203, INSERM U661, 34090 Montpellier, France.

[5] Laboratory of Functional Proteomics, INRA, 34000 Montpellier, France.

[6] Vanderbilt University, Tennessee 37235, USA

[7] Centre de Recherche de Biochimie Macromoléculaire, CNRS UMR5237, 34293 Montpellier, France.

[8] Present address: Institut Jacques Monod, CNRS UMR7592, University Paris Diderot, 75013 Paris, France

[9] Co-first author.

Contact information: * correspondence to: daniel.fisher@igmm.cnrs.fr

Running title: actin dynamics and DNA replication

Abstract

Nuclear actin influences transcription in a manner dependent on its dynamics of polymerisation and nucleocytoplasmic translocation. Using human somatic cells and transcriptionally-silent *Xenopus* egg extracts, we show that actin dynamics is also required for DNA replication. We identify many actin regulators in replicating nuclei from *Xenopus* egg extracts, and show that in human cells, nuclear actin filaments form in early G1 and disassemble prior to S-phase. In either system, treatments that stabilise nuclear actin filaments abrogate nuclear transport and initiation of DNA replication. Mechanistically, actin directly binds RanGTP-importin complexes and disruption of its dynamics hinders cargo release. This prevents both nuclear pore complex (NPC) formation and active nuclear transport, which we show is required throughout DNA replication. Nuclear formin activity is required for two further steps: loading of cyclin-dependent kinase (CDK) and proliferating cell nuclear antigen (PCNA) onto chromatin and initiation of DNA replication. Thus, actin dynamics and formins are involved in several nuclear processes essential for cell proliferation.

Keywords: DNA replication / nuclear transport / actin / formin / CDK

Introduction

In mammalian cells, various functions have been attributed to nuclear actin (Huet *et al*, 2012). Monomeric actin binds chromatin remodeling and RNA polymerase complexes (Rando *et al*, 2002; Kapoor *et al*, 2013) and promotes transcription by all three RNA polymerases (Hofmann *et al*, 2004; Hu *et al*, 2004; Philimonenko *et al*, 2004). Its nuclear levels are regulated by active transport between the nucleus and cytoplasm (Stüven *et al*, 2003; Dopie *et al*, 2012) and polymerisation (Baarlink *et al*, 2013; Lundquist *et al*, 2014; Vartiainen *et al*, 2007). This dynamics is complex: monomeric actin promotes export of the serum response factor (SRF) cofactor MAL/MRTF, extinguishing SRF, yet both nuclear actin polymerisation (Baarlink *et al*, 2013) and depolymerisation (Lundquist *et al*, 2014) can induce SRF-dependent transcription. In epithelial cells, loss of nuclear actin triggers quiescence by disrupting binding of RNA polymerases to their transcription sites (Spencer *et al*, 2011). Nuclear actin also affects co-repressor eviction from promoters (Huang *et al*, 2011) and it can bind to gene regulatory regions (Miyamoto *et al*, 2011; Miyamoto *et al*, 2013a).

In vitro, purified actin and profilin self-assemble into long filaments, but cells additionally require actin nucleation factors. Sub-populations of nuclear actin have distinct mobilities, suggesting existence of polymeric forms (Dopie *et al*, 2012; McDonald *et al*, 2006), and several regulators of actin polymerisation have been found in nuclei (Khoudoli *et al*, 2008; Miyamoto *et al*, 2013b; Obrdlik & Percipalle, 2011; Wu *et al*, 2006; Yoo *et al*, 2007; Dopie *et al*, 2015). Physiological nuclear actin polymerisation remains poorly characterised due to difficulties in staining nuclear actin with phalloidin (Grosse & Vartiainen, 2013). In specific settings, like the giant non-replicating nuclei of amphibian oocytes, a filamentous actin network has scaffolding functions (Clark & Rosenbaum, 1979; Gounon & Karsenti, 1981; Feric &

Brangwynne, 2013). Stabilised nuclear actin filaments are observed in several pathologies (Lanerolle, 2012) and can be induced by various manipulations, including heat shock and DMSO treatment (Iida *et al*, 1986; Sanger *et al*, 1980); increasing nuclear actin concentrations (Stüven *et al*, 2003; Kalendová *et al*, 2014); activation of nuclear mDia formin (Baarlink *et al*, 2013); overexpression of NLS-tagged IQGAP1 (Johnson *et al*, 2013) or supervillin (Serebryannyy *et al*, 2016); or knockdown of MICAL-2, which promotes nuclear actin depolymerisation through methionine oxidation (Lundquist *et al*, 2014). Stabilisation of nuclear actin filaments inhibits transcription by RNA polymerase II (Serebryannyy *et al*, 2016), whereas serum stimulation of mouse fibroblasts triggers transient nuclear actin filament formation, promoting SRF-dependent transcription (Baarlink *et al*, 2013).

We investigated whether nuclear actin has transcription-independent roles in cell proliferation by using transcriptionally silent *Xenopus* egg extracts (XEE). This system recapitulates early embryonic cell cycles *in vitro*, allowing identification of nuclear assembly pathways (Hetzer *et al*, 2005) and DNA replication mechanisms (Arias & Walter, 2004). Using XEE as well as human somatic cells, we show that actin dynamics is required for initiation of DNA replication, through at least two mechanisms: first, actin dynamics is required for nuclear transport, as polymeric nuclear actin locks cargo-importin-Ran complexes, preventing cargo release from importins. Second, nuclear formin activity promotes chromatin loading of DNA replication factors allowing initiation of DNA synthesis.

Results

Nuclear actin dynamics during the cell cycle

We first analysed the combined nucleoskeleton and chromatin proteome of nuclei assembled in XEE by label-free high-resolution mass spectrometry. To assess possible cell cycle regulation of nuclear assembly, we compared replicating nuclei with nuclei assembled in the presence of purvalanol A (PA) to inhibit CDKs (Echalier *et al*, 2012) (Fig 1A). We identified 2610 non-redundant proteins (Fig 1B, C; Supplementary Figure 1, S1). Enriched biological processes included DNA metabolism, chromatin organisation, and, interestingly, regulation of actin polymerisation (Fig 1D; Table S2). We identified 55 actin regulators (Tables S3 & S4), including actin filament nucleating factors such as formins and the Arp2/3 complex. These were unaffected by CDK activity, unlike chromatin recruitment of proteins involved in DNA replication, DNA repair and the S-phase checkpoint (Fig 1B-E; and Tables S1&2). Immunofluorescence analysis confirmed that many actin polymerisation regulators localised to replicating nuclei (Fig 2A), where actin was mostly insoluble (Fig 2B). To visualise nuclear actin directly, we added trace concentrations of fluorescently-labeled actin protein to XEE. This revealed filaments in the egg cytosol, as expected, and both diffuse and patterned intra-nuclear staining (Fig 2C-E). The latter might be actin polymers or monomeric actin associated with other structures, for example chromatin. Labelled DNase1, a high affinity G-actin probe, mainly stained chromatin (Fig 2F).

Next, we investigated possible cell cycle regulation of endogenous nuclear actin dynamics in living cells with an actin chromobody (Chromotek®) modified by the addition of a nuclear localisation signal (NLS – see materials and methods). An identical tool was independently developed recently (Plessner *et al*, 2015). We concurrently followed the DNA replication programme using a second chromobody to visualise endogenous PCNA (Burgess *et al*, 2012). Interestingly, we found that a

dynamic network of actin filaments formed in most early G1-nuclei (Fig 2G). Filaments disassembled after an average of 200 minutes, in mid-late G1 (Fig 2H; Movie 1). These G1 actin filaments could be stained with phalloidin (Fig 2G), which, importantly, also labelled a G1 nuclear actin network in cells not expressing the chromobody (Fig 2I). Expressing Lifeact-GFP-NLS also revealed nuclear actin filaments (Supplementary Figure 2A). However, this probe disrupted nuclear actin dynamics as although the filaments appeared in G1, they became longer and stable and cells did not divide (Movie 2).

In mouse fibroblasts, formins promote formation of nuclear actin filaments in the serum response (Baarlink *et al*, 2013). Specific formin inhibition with SMIFH2 (Rizvi *et al*, 2009) induced stabilisation of long nuclear actin filaments or patches in the majority of cells (Supplementary Figure 2B, C; Movie 3,4). The former is similar to the effect of formin inhibition on actin dynamics in a reconstituted *in vitro* system (Rizvi *et al*, 2009), and suggests that SMIFH2 stabilised long nuclear actin filaments by preventing formin-mediated nucleation of new filaments, coupled with formin-independent elongation of existing ones.

We subsequently employed XEE to investigate effects of modifying actin dynamics on nuclear actin independently of cytoskeleton-environment interactions and of transcription. First, we used recombinant actin regulatory proteins, as well as different drugs that modify actin dynamics, in preassembled nuclei in XEE (Fig 3A, B). Cytochalasin D (CytD), jasplakinolide, or purified Arp2/3 and GST-WASP-VCA proteins all strongly increased total nuclear actin, which was mostly insoluble. The effects of CytD, which binds the barbed (plus)-end of F-actin, arresting both polymerisation and depolymerisation at the plus end (Schliwa, 1982), were reversed by latrunculin A that potently binds actin monomers, impeding filament assembly.

Interestingly, Cyt D caused formation of stable nuclear actin filaments that were visualised with phalloidin (Fig 3C). These data suggest that nuclear actin polymerisation and depolymerisation exist in a dynamic equilibrium in XEE.

Actin dynamics is required for DNA replication

We next assessed the effect of these manipulations of actin dynamics on DNA replication. S-phase entry in G1-synchronised cells was dose-dependently inhibited by SMIFH2 (Fig 4A; Supplementary Figure 3A, B), and PCNA binding to chromatin was reduced (Supplementary Figure 3C). SMIFH2 also abolished general transcription, as determined by 5-ethynyl-uridine (EU) incorporation into newly synthesized RNA (Fig 4B; Supplementary Figure 3D). We then altered endogenous formin activity by expressing GFP-tagged mDia2 diaphanous autoregulatory domain (DAD), either specifically in the nucleus (GFP-DAD.LG.NLS) or cytoplasm (GFP-DAD). Interestingly, neither mDia2-DAD construct interfered with global transcription (Fig 4C). Nuclear, but not cytoplasmic, mDia2-DAD increased the fraction of cells in S-phase (Fig 4D, left), implying that over-activating nuclear formins impedes S-phase progression in a transcription-independent manner. To test whether this might be due to aberrant nuclear actin dynamics, we expressed the nuclear-localised actin mutants S14C and G15S, that favour polymerisation, or the polymerisation-defective R62D) (Supplementary Figure 3E). WT and R62D mutants had no effects on S-phase, but, like formin activation, S14C and G15S mutants increased the fraction of cells in S-phase (Fig 4D, right) and decreased EdU signal intensity (Fig 4E). Thus, promoting nuclear polymeric actin or derepressing formins both impede S-phase progression. Treatment with SMIFH2 of cells expressing PCNA chromobody increased by ten-fold the duration of individual PCNA foci (Fig 4F; Movie 5). Likewise, overexpression of

GFP-DAD.LG.NLS immobilised PCNA foci (Movie 6). Impaired PCNA mobility might indicate replication fork stalling, which can generate DNA damage. Indeed, expression of nuclear DAD constructs or SMIFH2 treatment led to formation of DNA double-strand breaks, as shown by the increase in the number of γ-H2AX-positive cells (Supplementary Figure 3F, G). Thus, actin and formin constructs that specifically disrupt nuclear actin dynamics hinder DNA replication.

To assess possible effects of altered nuclear actin dynamics on DNA replication independently of transcription, we used XEE. Arresting actin dynamics with CytD inhibited DNA replication (Fig 4G). Combining CytD with jasplakinolide or gelsolin protein was synergistic (Supplementary Figure 4A), whereas latrunculin A, or recombinant cofilin, which severs actin filaments and dissociates monomers, rescued replication (Fig 4H; Supplementary Figure 4B). Inhibiting formins using SMIFH2 or compound 2.4 (Gauvin *et al*, 2009), or inhibiting Arp2/3 with CK-666 (Nolen *et al*, 2009) but not its inactive analogue, CK-689, also blocked DNA replication, as did recombinant MICAL2 protein (Fig 4I; Supplementary Figure 4C-E). Taken together, these results indicate that actin dynamics is required for DNA replication in XEE, independently of transcription. Disrupting actin dynamics inhibited conversion of pre-replication complexes containing ORC and MCMs to pre-initiation complexes (pre-IC) containing Cdc45 and PCNA (Fig 4J; Supplementary Figure 4F). We thus tested possible interactions of endogenous actin with replication factors PCNA, MCMs and RPA by Proximity Ligation Assay (PLA). We could readily detect sites of DNA replication by PLA. Actin interacted with PCNA, but not with RPA or MCMs, indicating that it is not present at replication sites (Supplementary Figure 4G, H). Actin physically associated with PCNA, as confirmed by pulldowns from nuclei using immobilised actin-binding peptide Lifeact (Supplementary Figure 4I).

Actin dynamics is required for NPC formation and nuclear transport

In XEE, inhibiting actin dynamics prevented DNA decondensation and growth of nuclei (Fig 5A), while nuclei in SMIFH2-treated U2OS cells were smaller and misshapen (Fig 5B). These observations suggested that actin dynamics might be required for nuclear assembly or transport, both of which are essential for DNA replication. We therefore examined nuclear pores in XEE by 3D structured illumination microscopy and whole-mount field-emission scanning electron microscopy (FEISEM). Upon SMIFH2 treatment, nucleoporin (NUP) staining was disorganised, with dense NUP clusters between NUP-free regions (Fig 5C). While most NUPs were present, NUP160 was undetectable, and the levels of NUP107, Gp210, NUP358, NUP214 and NUP183 were decreased (Supplementary Figure 5A). Furthermore, in nuclei formed in the presence of SMIFH2 or CytD, we could not detect nuclear pores with electron microscopy (Fig 5D).

We next tested nuclear transport using NLS-tagged GST-GFP. In nuclei formed in CytD- or SMIFH2-treated extracts, the nuclear membrane was intact, but the probe did not accumulate inside nuclei (Fig 6A; Supplementary Figure 5B). Early steps in NPC assembly were unaffected as Elys, importin β, FG-NUPs and RCC1 all bound DNA with similar kinetics to controls (Supplementary Figure 5C). The subsequent step involves RanGTP-mediated release of nucleoporins from importin-β (Bai *et al*, 2014). Since the same mechanism also governs active nuclear transport through mature NPCs, we assessed effects of modifying actin dynamics on nuclear transport in preassembled nuclei with NLS-tagged GST-GFP (Fig 6B, scheme). We used wheat germ agglutinin (WGA) that blocks NPC function and importazole that disrupts Ran-importin-β interaction (Soderholm *et al*, 2011), and

inhibited CDK with PA, which blocks DNA replication without affecting NPC function. As expected, importazole blocked DNA replication (Supplementary Figure 5D). Neither CytD nor SMIFH2 affected integrity of pre-formed NPCs, as assessed probing passive transport with fluorescently labeled dextrans (Mohr *et al*, 2009) (Supplementary Figure 5E). Nevertheless, disrupting actin dynamics abolished nuclear transport, as did WGA and importazole, whereas PA had no effect (Fig 6B).

We next investigated whether actin dynamics is required for importin-dependent nuclear transport in human cells. We analysed nuclear translocation of endogenous NF-κB (Transcription factor p65) in primary human fibroblasts upon stimulation with IL-1β (Interleukin-1 beta) or TNFα (Tumour necrosis factor alpha). Treatment with the cytokines releases NF-κB from its inhibitor IκB (I-kappa-B) and triggers its nuclear translocation, thus bypassing possible effects of cytoplasmic actin disruption on cell shape and NF-κB regulation (Németh *et al*, 2004; Sero *et al*, 2015). This allowed us to study effects of CytD or formin inhibition on NF-κB nuclear translocation itself. Importazole, as expected, strongly reduced NF-κB nuclear translocation. CytD had only a moderate effect, probably because it strongly affected cell shape, which has been reported to alter cytoplasmic NF-κB regulation (Németh *et al*, 2004; Sero *et al*, 2015). In contrast, SMIFH2 did not significantly change cell shape, but almost completely abolished NF-κB nuclear translocation (Fig 6C, D).

Arresting actin dynamics hinders cargo release from importin

Next, using XEE, we investigated the mechanism whereby inhibiting actin dynamics disrupts nuclear transport. Since FG-NUPs are cargo of importin-β during NPC formation in extracts, we compared FG-NUP-importin interactions in control and CytD- or importazole-treated extracts. Both treatments increased binding of importins

to FG-NUPs (Fig 7A). We then analysed effects of CytD and SMIFH2 on binding of importin-β to cargo in nuclei. We immunoprecipitated FG-NUPs from nuclear extracts and immunoblotted for PCNA, as well as an unrelated cargo, TPX2 (Targeting protein for Xklp2-A). Importantly, SMIFH2 treatment severely decreased the abundance of all tested proteins in the nuclei. Both treatments resulted in loss of PCNA from nuclei, suggesting that nuclear import of PCNA no longer counterbalances its export. CytD but not SMIFH2 strongly increased the NUP-actin interaction (Fig 7B). PCNA and TPX2 bound similarly to NUPs, indicating that cargo binding is not altered by actin. We then tested whether cargo release in the nucleoplasm was affected. This depends on productive Ran-importin interactions (Lowe *et al*, 2010). Ran binding to importin-β and RCC1, its GTP exchange factor, was not altered by CytD or SMIFH2. However, CytD strongly promoted actin-Ran interaction and TPX2 remained bound to importin-β, suggesting that increased actin binding might hinder cargo release (Fig 7C). TPX2 could not be detected in pull downs from nuclei with SMIFH2, probably as a result of its elimination from the nucleus. Actin binding to Ran could be reconstituted with purified proteins (Fig 7D), and it was independent of whether Ran was in its GDP- or GTP-loaded form (Fig 7E). CytD had no effect on RanGTP levels but promoted nuclear RanGTP-actin binding, and latrunculin A reversed this phenotype (Fig 7F). SMIFH2 marginally increased actin binding to RanGTP, an effect similarly cancelled by latrunculin A. These results suggest that treatments that increase actin binding to RanGTP prevent cargo release from importins, but that this is independent of alterations of nuclear actin levels.

Formins act in parallel with CDK to promote pre-IC formation

While nuclear transport is required for nuclear assembly and S-phase onset, our results in human cells indicated that inhibiting formins impairs DNA replication even after nuclear assembly. It was thus important to discriminate whether the roles of formins in DNA replication were exclusively due to their requirement for NPC formation and function. If so, it would suggest that there is a continued requirement for nuclear transport throughout DNA replication. To address this question, we determined execution points for biochemical activities at successive phases of DNA synthesis. We thus used XEE and performed nuclear transfer experiments in which nuclei were isolated from one extract and transferred to another with different conditions. We first used WGA to block existing NPC function, or prevented new NPC formation by depleting nucleoporins with WGA (WGA-bpΔ). As expected, both treatments blocked DNA replication (Supplementary Figure 6A, B). We then combined these treatments with nuclear transfers. Nuclei were formed in an extract where replication licensing was prevented by adding recombinant geminin (Fig 8A, scheme; Supplementary Figure 6C). These nuclei were then transferred into a second extract with added recombinant Cdt1, to release the licensing block, and containing SMIFH2, WGA or vehicle, or depleted of NUPs. In nuclei transferred into NUP-depleted extract, DNA replication occurred, albeit less efficiently (Fig 8A, WGA-bpΔ). However, replication was totally blocked by the further addition of SMIFH2 (Fig 8A, WGA-bpΔ +SMIFH2). Blocking existing NPCs with WGA also prevented replication (Fig 8A, +WGA). Therefore, once nuclei have been correctly formed, DNA replication can initiate in the absence of further NPC formation, but not if formins or existing NPCs are inhibited.

This suggests that formins might have a role in the continued function of NPCs in DNA replication. To further investigate such a possibility, we used a double

reciprocal nuclear transfer. First extracts contained geminin and second extracts contained either SMIFH2 or WGA. Nuclei were further transferred into a third extract with the alternative condition or to a control extract (scheme, Fig 8B). Neither transfer from WGA-into-SMIFH2, nor from SMIFH2-into-WGA allowed DNA replication in the third extract (Fig 8B). Therefore, ongoing nuclear transport and formin activity are required to promote DNA replication in fully formed nuclei.

Given that CDK activity is essential for pre-IC formation, but not for nuclear assembly or transport, we next performed reciprocal nuclear transfer between CDK-inhibited (PA) and WGA-treated extracts. Replication was abolished when nuclei were transferred from PA to WGA (Supplementary Figure 6D), confirming that active nuclear transport is required in parallel with CDK to promote pre-IC formation. Assuming formin function is to allow nuclear transport, formin activity should therefore be essential for pre-IC formation. We tested this by transferring nuclei from geminin-containing extract to a second extract, treated with either PA, SMIFH2 or vehicle, and quantifying DNA replication. As expected, both PA and SMIFH2 prevented replication in preassembled nuclei (Fig 8C). Chromatin-bound PCNA was essentially undetectable in SMIFH2-treated nuclei (Fig 8D), showing that formin activity is required after nuclear assembly in XEE to allow pre-IC formation and DNA replication, as in somatic cells. We therefore next determined whether formins and CDK act sequentially or in parallel. We performed reciprocal nuclear transfer experiments between a formin-inhibited and a CDK-inhibited (PA) extracts (Fig 8E). First extracts additionally contained aphidicolin to prevent replication fork progression, so that replication in the second extract reflected pre-IC assembly. DNA replicated when transferred from a control first extract to a second containing SMIFH2 or PA, but not when transferred from PA to SMIFH2, nor, as expected, when

316 transferred from SMIFH2 to PA (Fig 8E). Therefore, formins are required in parallel
317 with CDK to promote pre-IC formation.
318
319 **Nuclear formin activity controls chromatin loading of PCNA and CDKs**
320 Finally, we tested whether nuclear formins might have roles in DNA replication that
321 are independent of nuclear transport. To do this, we performed a nuclear transfer
322 experiment where first extracts contained leptomycin B to inhibit the exportin Crm1,
323 allowing nuclear accumulation of replication factors, and PA to inhibit initiation of
324 replication. Second extracts contained SMIFH2 or vehicle, with or without leptomycin
325 B (Fig 9A). DNA replicated efficiently in control second extracts. Without leptomycin
326 B in the second extract, SMIFH2 treatment decreased nuclear levels of both CDKs
327 and PCNA, explaining why continuous nuclear transport is required for efficient DNA
328 replication. Leptomycin rescued CDK and PCNA levels, but DNA still could not
329 replicate (Fig 9B), and neither CDK nor PCNA were present on the chromatin (Fig
330 9C). Therefore, nuclear formin activity is further required for loading of pre-IC
331 components onto chromatin. Decreased loading of PCNA would lead to reduced
332 origin firing and fork stalling, which would explain impaired S-phase progression
333 observed in somatic cells and induction of DSBs (Fig 4D-F; Supplementary Figure
334 2A-C, F,G).
335 We surmised that chromatin loading of PCNA and CDK, as well as DNA
336 replication, might not require formins in nucleoplasmic extracts (NPE). They are
337 highly concentrated and DNA can replicate in the absence of a nuclear envelope
338 (Walter *et al*, 1998). DNA in control NPE replicated efficiently, but replication was
339 totally abolished when formin activity was inhibited with SMIFH2 (Fig 9D). A similar
340 effect was observed with the 2.4 formin inhibitor (Supplementary Figure 6E).

Importantly, the initial loading of PCNA and other pre-IC components onto chromatin occurred, but did not increase following initiation of DNA replication as in the control extract (Fig 9E). Thus, formin inhibition specifically prevents chromatin loading of replication components in nuclei, and reveals an additional downstream formin-dependent step in the initiation of DNA replication.

Discussion

Our study identifies new roles for actin dynamics and formins in controlling cell proliferation. There are several reasons why this might not previously have been observed. First, cell anchorage and the cytoskeleton are involved in growth factor-dependent transcription, *e.g.* of cyclin D1 in mammalian cells (Assoian & Zhu, 1997), as well as degradation of the CDK inhibitor CDKN1A (Densham *et al*, 2009). This is at least partly due to cytoplasmic MST kinase activation and signaling to JNK (Densham *et al*, 2009), obscuring possible effects of altered nuclear actin dynamics. We and others (Serebryannyy *et al*, 2016) find that treatments that induce nuclear actin filaments eliminate global transcription. We show here that manipulating nuclear actin also arrests DNA replication in a transcription-independent manner in somatic mammalian cells. Additionally, we found that specifically interfering with activity of nuclear formins in S-phase and actin dynamics disrupts DNA replication in transcriptionally silent XEE. Second, actin is required in other cell cycle phases, for cortical reorganisation and contractile ring formation (Schroeder, 1973), centrosome separation and mitotic spindle formation (Uzbekov *et al*, 2002; Rosenblatt *et al*, 2004). Thus, genetic mutation or knockdown of actin regulators, which cannot be induced specifically in S-phase, disrupt cell division. Identification of roles for actin dynamics in S-phase can only be achieved using chemical modulation in

366 synchronised cells, or using a system such as XEE where S-phase can be studied
367 independently of other cell cycle phases, transcription and the cytoskeleton, is
368 synchronous and can be broken down into individual steps.

369 Because XEE are highly concentrated compared to cell culture medium, and
370 there is no active drug transport, far higher concentrations of pharmacological
371 inhibitors are required than in cultured cells. XEE contain around 50 mg/ml protein, of
372 which 5-10% is actin. Thus, there is at least 100 µM actin in extracts. Since effective
373 drug concentrations depend on adsorption, distribution and metabolism, it is
374 expected that several hundred-micromolar concentration of actin drugs is required to
375 elicit phenotypic effects in this system. In contrast, in cells, due to active import,
376 drugs can routinely attain 1000-fold higher concentrations than in the medium
377 (Martinez Molina *et al*, 2013).

378 Nucleocytoplasmic shuttling of actin (Dopie *et al*, 2012) means that drug
379 effects on cytoplasmic actin have knock-on effects on nuclear actin levels. Indeed,
380 CytD and jasplakinolide both greatly increased nuclear actin levels, and CytD
381 promoted nuclear actin filament stabilisation in XEE. However, adding recombinant
382 GST-WASP-VCA and Arp2/3 also increased nuclear actin but did not promote similar
383 filament formation nor affect nuclear transport and DNA replication. Conversely,
384 formin inhibition did not raise nuclear actin levels nor trigger nuclear actin filament
385 stabilisation, yet inhibited both nuclear transport and DNA replication. Furthermore,
386 addition of purified proteins MICAL2 or gelsolin was inhibitory for replication, while
387 addition of recombinant cofilin could rescue the effects of CytD. Finally,
388 hyperactivation of nuclear formins inhibited S-phase progression. These results imply
389 that deregulated nuclear actin dynamics, rather than an increase in nuclear actin
390 levels or filament formation *per se*, prevents DNA replication.

Our experiments in XEE demonstrate that actin dynamics is essential both for NPC assembly and for nuclear transport, and we reveal one underlying mechanism. Both of these processes involve importin-α/β-mediated cargo binding and subsequent release, which is dependent on the interaction with Ran. Arresting actin dynamics results in increased actin binding to RanGTP, preventing cargo release from importin-β. A similar phenotype has been observed with importazole, which alters Ran-importin interactions without preventing their binding (Soderholm *et al*, 2011). Similarly, the K37D/K152A Ran mutation affects importin-β-Ran interactions, impeding cargo release (Lee *et al*, 2005). Future studies will be required to map the exact interaction sites and determine conformational changes induced by actin binding to Ran, and how this modifies Ran-importin interactions.

Further work will also be required to define whether the observed effects of altering formin activity can be entirely attributed to changes in actin dynamics. We find that activating endogenous nuclear formins in somatic cells, or favouring nuclear actin polymerisation by expressing NLS-tagged actin mutants, arrests ongoing DNA replication. We also find that formin activity is required for DNA replication downstream of nuclear assembly and independently of nuclear transport. In XEE it is required for loading CDKs and PCNA onto chromatin, while in NPE it directly promotes DNA replication. These results suggest that nuclear organisation is not simply required to concentrate replication factors, as assumed from DNA replication in nuclear envelope-free *Xenopus* nucleoplasmic extracts (Walter *et al*, 1998). It will be important to define the precise mechanism of these formin-dependent steps in DNA replication.

In conclusion, together with accumulating evidence for important roles in chromatin regulation and transcription, our study strongly reinforces the notion that actin dynamics and formins have critical effects on essential nuclear processes.

Materials and Methods

Antibodies

Antibodies used are as follows: XCdc45, XCdc6, XRPA, XMCM3, XCut5 (gifts from M. Méchali); XORC2, XMCM6 (gifts from J. Maller); XCut5 (gift from D. Maiorano); PCNA (Abcam; ab18197, or Oncogene Science NA03); PSTAIR (Sigma-Aldrich; P7962); human Cdc6 (H-304, Santa Cruz Biotechnology; SC-8341); actin (Sigma-Aldrich, clones A2066 or AC-15; Hypermol, clone 2G2); Ran (Santa Cruz Biotechnology, C29; SC-1156); active Ran (NewEast Biosciences; 26915); cofilin (Abcam; ab42824); Arp2 (Abcam; ab47654); mDia2 (One World Lab; 11016); NFκB p65 (A) (Santa Cruz Biotechnology; SC-109); XNUP107, XNUP62, XNUP153 (gifts from B. Heulsmann); Elys (gift from J. Blow); γH2A.X pSer129 (Millipore, clone JBW301); TPX2, XRCC1, HS importin β . In house rabbit polyclonal antibodies against His-tagged *Xenopus* importin α were raised and affinity purified. The original construct for His-tagged human importin-α was a gift of D. Goerlich; XLaminB3 (gift from B. Goldman); WASP (Abcam; ab74904); mAb414 (Abcam; ab50008); ROCK1 (Abcam; ab58305); Arp3 (Abcam; ab49671); Cortactin (Millipore; clone 4F11); tubulin (Santa Cruz Biotechnology; SC-9104); GST (Pierce; MA4-004); biotin (Cell Signaling; D5A7); digoxigenin (Roche, clone 1.71.256).

Plasmids

The PCNA-TagRFP and actin-TagGFP chromobodies were purchased from Chromotek ®. To allow endogenous nuclear actin detection, the SV40 nuclear localisation sequence (NLS, ccgcctaagaaaaagcggaaggtg) was added at the C-term of the actin chromobody, or in between the actin Vhh sequence and the TagGFP. The former is essentially identical to the nAC recently published (Plessner *et al*, 2015) but with a different stop codon. Both of our nuclear actin chromobodies gave identical results but only the former was used in this study. The actin-NLS R62D mutant (Baarlink *et al*, 2013) was used as template to generate the actin-NLS WT form and that was subsequently mutated to S14C or G15S. Formin mutants, mDia2-DAD constructs, actin-NLS R62D, and Lifeact-GFP-NLS were gifts from R. Grosse.

Xenopus egg extracts and replication reactions

Interphase egg extracts, chromatin isolation and replication assays were prepared and performed essentially as described (Blow & Laskey, 1986), with minor modifications. In brief, eggs laid overnight in 150mM NaCl were dejellied in degellying buffer (29mM Tris pH 8.5, 110mM NaCl, 5mM DTT); rinsed several times in High Salt Barths solution (15mM Tris pH 7.6, 110mM NaCl, 2mM KCl, 1mM MgSO4, 0.5mM Na2HPO4, 2mM NaHCO3), twice in MMR (5mM HEPES-KOH pH 7.6, 100mM NaCl, 2mM KCl, 0.1mM EDTA, 1mM MgCl2, 2mM CaCl2), before activation with 0.3µg/ml calcimycin ionophore in MMR. Subsequently, two rinses in MMR and two more in SB (50mM HEPES-KOH pH 7.6, 50mM KCl, 2.5mM MgCl2, 5% Sucrose, 0.014% β-mercaptoethanol) followed, while during the last rinse the eggs were transferred on ice and SB was supplemented with protease inhibitors (10µg/ml leupeptin, pepstatin and aprotinin). Eggs were spun down at 200g for 1min and excess of buffer removed before being centrifuged at 16,000g, 4°C for 10

463 minutes. Protease inhibitors and 10µg/ml cytochalasin B were added to the
464 cytoplasmic fraction. This concentration of cytochalasin B, a much weaker actin drug
465 than cytochalasin D, is required to reduce the viscosity sufficiently that extracts can
466 be obtained by centrifugation but has no effect on DNA replication and does not
467 provoke nuclear actin stabilisation. Extracts were further centrifuged in SW55Ti rotor
468 for 20min at 20k rpm (48,000g) at 4°C. The cytoplasmic layer was extracted with a
469 large-bore needle and syringe, and supplemented with glycerol 3% and ATP
470 regenerating system (10mM creatine phosphate, 10µg/ml creatine kinase, 1mM ATP,
471 1mM MgCl2) added from a 20x stock. Aliquots were frozen in liquid nitrogen. Where
472 indicated, a 1:100 dilution of cytochalasin D (at final concentration of 400 µM, unless
473 otherwise indicated; Enzo); SMIFH2 (500 µM, unless otherwise stated; Calbiochem);
474 Purvalanol A (200 µM; Sigma-Aldrich); latrunculin A (100 µM, unless otherwise
475 indicated; Enzo); jasplakinolide (100 µM; Enzo); importazole (500 µM, unless
476 otherwise indicated; Sigma-Aldrich); 2.4 formin inhibitor (at indicated concentrations;
477 K216-0385, ChemDiv); CK-666 or CK-689 (Calbiochem), or DMSO solvent only was
478 added to the *Xenopus* egg extracts. Where indicated, extract was supplemented
479 with: recombinant geminin and Cdt1 (40nM; gift from M. Lutzmann); recombinant
480 MICAL2 (48ng/µl of extract; gift from V.N. Gladyshev); WGA (0.2 mg/ml;
481 Calbiochem); aphidicolin (25 µg/ml; Sigma-Aldrich); recombinant cofilin (5 µM;
482 Hypermol; 8419-01); recombinant Arp2/3 complex and GST-VCA (200nM; Hypermol;
483 84101 and 8416-01, respectively); recombinant His-Ran WT and Q96L (used at 5µM;
484 purified as described previously: (Bompard et al., 2005); gelsolin (80ng/µl; Sigma-
485 Aldrich, G8032); dextran-Alexa Fluor 488 10,000MW, and dextran-Rhodamine B
486 70,000MW (used at 2.5µl/µl; Life Technologies, D-22910 and D-1841). For mass
487 spectrometry analysis, sperm heads were added at concentration of 2800/µl and the

insoluble fraction of nucleoskeleton and chromatin was isolated at 50 min from 1ml of extract per condition. Nucleoplasmic extracts (NPE) preparation, analysis of DNA replication efficiency and chromatin loading of replication factors were performed as described . *Chromosomal DNA replication in a soluble cell-free system derived from Xenopus eggs*, AV Tutter and JC Walter, in *Xenopus Protocols. Cell Biology and Signal Transduction*. Humana Press, Totowa, New Jersey 2006). The NPE was supplemented with DMSO, SMIFH2 or 2.4 compound at 1.6% (SMIFH2 final concentration 800µM, unless otherwise stated).

Cell culture

Cells (U2OS or HeLa) were cultured in DMEM Glutamax (Invitrogen) supplemented with 10% heat inactivated Fetal Bovine Serum (FBS; Invitrogen) and 1x antibiotic mixture (complete medium). Cell lines were tested for mycoplasma contamination regularly. For cell cycle synchronisation, cells were incubated in complete medium containing 2 mM thymidine for 14-16 h. After an 8-10 h release in complete medium, 2 mM thymidine was added again for 20 h. Cells were released and 6-7 h later nocodazole (50-100 ng/mL) was added for additional 5 h. Cells were washed with PBS and complete medium was added for 4.5 h, at which time DMSO or SMIFH2 (50 µM) was added. At indicated time-points, cells were detached by trypsinisation, washed with ice-cold PBS and pellets were collected for FACS and/or immunoblotting analysis. For transient transfections of plasmid DNA, jetPEI or Lipofectamine 2000 or 3000 was used, according to the manufacturer's instructions (Polyplus Transfection or Invitrogen, respectively).

U2OS cells stabely expressing the nuclear actin or PCNA chromobody were obtained upon Lipofectamine-2000 transfection and selection with 2 µg/ml pyromycin. Clones were obtained by serial dilution.

To analyse NFκB translocation, RA-FLS (rheumatoid arthritis, fibroblast-like synovicites) were prepared as described (J. Morel et al. JBC 2005; 280: 15709-18) (Morel *et al*, 2005). Cells were seeded at 10 000 per well on coverslips in 12-well plates in RPMI medium/5% FBS, allowed to adhere for 24hrs, then starved overnight in RPMI/1% FBS. The following day, fresh medium/1% FBS was supplemented with 0.1% DMSO, importazole (50µM) or SMIFH2 (50µM) for one hour, followed by stimulation with IL-1β (10ng/ml final; Miltenyi Biotec) or TNF-α (10ng/ml final; Miltenyi Biotec) for 30 min. Cells were then washed in PBS, fixed in 3.7% formaldehyde/PBS and proceeded for NFκB immunostaining.

Immunoprecipitations, pull-downs and nuclear transfers

Glutathione-immoblised GST-Ran wild-type and Q69L mutant were produced as previously described (Bompard *et al*, 2010). For IPs, 10µl of beads (glutathione-Sepharose (GE Healthcare) beads were used as Mock) were washed in PBS and incubated with lysed nuclei (corresponding to 25µl of extract, lysed at 55min; drugs were added at 40min) for 2h at 4°C, washed in 150mM NaCl/PBS, resuspended in Laemmli buffer and analysed by Western-blotting.

For mAb414 and importin-β IPs from egg extract, 10µl of DynaBeads (for mAb414) or 10µl packed protein G-agarose (Roche) beads (for importin-β) were washed with PBS and incubated with antibody for 2h at 4°C, subsequently washed in PBS and incubated with 25µl extract diluted with SB buffer for 2h at 4°C. Beads were then processed as above.

For anti-active Ran IP, 10µl packed protein G-agarose (Roche) beads were incubated with 1µg of antibody for 2h at 4°C, blocked in 10mg/ml BSA/PBS, washed in PBS and incubated with lysed nuclei (corresponding to 25µl of extract) for 2h at 4°C, washed in 0.1% Triton-X 100 / 150mM NaCl / PBS, resuspended in Laemmli buffer and analysed by Western blotting. For actin-Ran *in vitro* pull-down, glutathione-Sepharose (GE Healthcare) beads were pre-incubated with recombinant GST protein (Bompard et al. 2010); 10µl of glutathione-GST and glutathione-GST-Ran beads were washed and blocked in 10mg/ml BSA/PBS, washed in PBS and incubated with 1µg of actin-biotin (Cytoskeleton) for 2h at 4°C, then proceeded as above. For Lifeact-NLS-actin pull-down, 10µl packed Streptavidin-Agarose (Novagen) beads were incubated with 5 nmol Lifeact-NLS-biotin peptide (MG-VADLIKKFESISKEEGDPP-VATPPKKKRK-V-biotin; synthesised by Cambridge Research Biochemicals) for 2h at 4°C, washed in PBS and incubated with lysed sonicated nuclei (corresponding to 40µl of extract) for 2h at 4°C, washed in 150mM NaCl/PBS, resuspended in Laemmli buffer and analysed by Western blotting.

GTP/GDP nucleotide exchange assay with glutathione-immoblised recombinant GST-Ran was performed as previously described (Bompard et al., 2010). Beads were subsequently washed in wash buffer (20mM Tris pH 7.5, 50mM NaCl, 5mM MgCl2) and incubated with 1µg of actin-biotin (Cytoskeleton) / 10µl of beads for 2h at 4°C; washed in wash buffer, resuspended in Laemmli buffer and analysed by Western blotting.

For nuclear transfer experiments, sperm heads were added to egg extract supplemented as indicated, and at time points indicated, nuclei were diluted 10x in CPB buffer (50mM KCl; 20mM HEPES pH 7.6; 2% Sucrose; 5mM MgCl2) with protease inhibitors, layered onto 1ml sucrose cushion (0.7M Sucrose in CPB) and

561 centrifuged for 5 min. at 6,000g at 4°C, and resuspended in the recipient extract. For
562 nuclear fractionation, the pellet was further resuspended in CPB containing 0.3%
563 Triton-X 100, then recentrifuged, supernatant recovered as nucleoplasmic fraction
564 and pellet resuspended directly in Laemmli buffer as insoluble nuclear fraction. For
565 immunoblot analysis, fractions corresponding to the same number of nuclei were
566 loaded on gel.
567
568 **Immunofluorescence microscopy**
569 Immunofluorescence microscopy using *Xenopus* egg extract nuclei and preparation
570 of samples for visualizing actin was performed as described (Krauss *et al*, 2003).
571 Where indicated, 20 µM biotin-dUTP or digoxigenin-dUTP (Roche), and inhibitors or
572 DMSO, were used. Actin-Alexa Fluor and actin-biotin conjugates were obtained from
573 Life Technologies and Cytoskeleton, respectively, and used at 25 µg/ml. DHCC was
574 used at 2 µM. pGEX 4T1 GST-GFP-NLS plasmid was a gift from Dale Shumaker
575 (Northwestern University, Chicago) (Moore M. S., 2000). DNA was stained with 1
576 µg/ml Hoechst 33258. TRITC- or rhodamine-conjugated phalloidin (Invitrogen) was
577 used at 1/500. Secondary antibodies and Streptavidin were Alexa Fluor conjugates
578 and were used at 1/500. Images were taken with upright Zeiss AxioimagerZ1 (100x;
579 1.4NA) microscope operated with Metamorph 6.2.6. software (Molecular Devices),
580 using constant exposure time for each filter setting. Superresolution images were
581 taken using 3D-SIM with a Deltavision OMX microscope, with Olympus UPSLAPO oil
582 objective (100x; 1.4NA), and analyzed using OMERO.insight application. Confocal
583 images were taken using Leica SP5-SMD microscope. The Duolink in situ PLA was
584 performed according to the manufacturer's instructions (Olink Bioscience, Uppsala,
585 Sweden).

Cultured cells were seeded on gelatin-coated coverslips, synchronised and treated as described for each experiment. EdU (5-ethynyl-2´-deoxyuridine; 10 µM) or EU (5-ethynyl-uridine; 1mM for 1hr) were detected with click reaction using the Alexa Fluor® 647 Imaging Kit, according to the manufacturer's instructions (Invitrogen), and images were acquired as described above using constant exposure time between the tested conditions. For nuclear actin imaging, cells were transfected and fixed 24-48 hrs later either with 3.7% formaldehyde in cytoskeleton buffer (10 mM MES, 150 mM NaCl, 5 mM EGTA, 5 mM glucose and 5 mM MgCl2) at pH 6.2 (Small *et al*, 1999), or with glutaraldehyde essentially as described (Baarlink *et al*, 2013). TRITC-conjugated phalloidin was used at 1/1,000 for 1.5 hr. For "phalloidin alone" staining, cells were fixed with glutaraldehyde as above, and phalloidin was used at 1/200 for 20 min (for) after 3 quenching steps with sodium borohydride (1 mg/ml) (Small *et al*, 1999). Coverslips were mounted with DAPI-containing Prolong Gold or Diamond (Thermo Fisher). Image analysis, γH2A.X foci counting and signal intensity measurement was performed in Fiji-ImageJ (Schindelin *et al*, 2012) using identical parameters for all conditions. The NucleusJ plug-in (Poulet *et al*, 2015) was used to measure parameters of nuclear morphology.

For the analysis of NFκB translocation, images were acquired using a Carl Zeiss AxioimagerZ2 microscope, a plan-apochromat 40x 1.4 NA oil immersion lens and FS49 (Hoechst) and FS45 HQ (Texas Red) fluorescence filter sets, and a grid projection illumination system (aka. Apotome). The high signal to noise ratio and out of focus removal proved to be important for the analysis.

To increase the sample size, a large-field Hamamatsu Orca Flash4.0 LT sCMOS camera was used and 5x5 mosaic acquisitions were performed.

Individual tiles were analysed using a custom-designed Cell Profiler analysis routine.

Briefly, nuclei masks were identified using an intensity-based automatic Otsu threshold on the Hoechst images. Cut objects at the edges of the image, as well as non-nuclear small objects were discarded. Rare, fused nuclei were segmented using an intensity algorithm. Subsequently, the nuclear masks were expanded by 10 pixels. NFKB staining integrated intensity and masked areas were then measured in both nucleus and expanded nucleus masks. Cytoplasm integrated intensities and areas were derived using expanded nucleus mask minus nucleus mask values. Mean intensity values (integrated intensity/area) and nucleus/cytoplasm mean intensity ratios were calculated.

Statistics

Graphs were created and statistical analyses (two-tailed unpaired *t*-test) were performed in Microsoft Excel 2011 or GraphPad Prism 6. The number of cells counted in each condition and *P*-values (*, p≤0.05; **, p≤0.001; ***, p≤0.0001) are indicated in the figures. Duration of nuclear actin network and replication foci were measured manually and outliers were removed with the ROUT method (Q= 1%) in Prism 6.

Timelapse microscopy

For live videomicroscopy, cells were seeded in glass bottom 35 mm dishes with 1 or 4 compartments, transfected as above, and image analysis was initiated 10-15 min after addition of drugs. Z-stacks (10 µm in 5 planes) were acquired every 10 minutes using an inverted microscope (Nikon) equipped with confocal spinning disk CSU-X1 Andor, 60x/1.4 oil objective using the software Andor iQ3. Stacks were processed

635 and movies generated in Fiji. To measure the duration of nuclear actin network and
636 PCNA foci, timelapse videos with images taken at 10-min intervals were used.
637
638 **Electron microscopy**
639 Ten or twenty microliters of interphase *Xenopus* egg extract was supplemented with
640 sperm DNA as described above; nuclei were allowed to assemble in the presence or
641 absence of actin inhibitors (SMIFH2 or cytochalasin D). Sample preparation for
642 scanning electron microscopy (SEM) was performed as described (Allen *et al*, 2007),
643 with minor modifications. Briefly, reactions were stopped by diluting 25-fold with cold
644 CPB buffer supplemented with protease inhibitor cocktail (Sigma-Aldrich) and
645 centrifuged at 1,000 x g for 2 min at 4°C. Nuclei were resuspended in 0.5 ml CPB,
646 layered onto 0.5-1 ml sucrose cushion (0.7 M in CPB) and centrifuged at 3,000 x g
647 for 15 min at 4°C onto acetone-washed silicon chips (Agar Scientific). Nuclei were
648 fixed in fixation buffer (80 mM PIPES, pH6.8, 30mM KCl, 1mM MgCl2, 0.25%
649 glutaraldehyde, 2% formaldehyde, 5% w/v Sucrose) for 30 min at room temperature,
650 washed in 0.2 M sodium cacodylate, and post-fixed with 1% osmium tetroxide
651 solution in 0.2 M sodium cacodylate. After a wash in H_2O, samples were dehydrated
652 with increasing concentrations of ethanol (30%, 50%, 70%, 90%, and three times in
653 absolute ethanol) followed by 10-min incubation in graded ethanol –
654 hexamethyldisilazane. After one wash with hexamethyldisilazane, the samples were
655 sputter-coated with approximately 3-10nm thick gold film and examined under a
656 scanning electron microscope (Hitachi S4000 or S4800). Images were obtained
657 using a lens detector with an acceleration voltage of 20kV at calibrated
658 magnifications, with Axone software (version 2013; Newtec) and processed in
659 ImageJ or Photoshop.

660

661 **Fluorescence-activated cell sorting (FACS) analysis**

662 Cells (0.5-1 x 10^6) were suspended in cold PBS, then pure ethanol was added to
663 reach 70% (v/v) and fixed cells were stored in -20°C until FACS analysis. DNA was
664 stained in PBS solution containing 2.5 µg/ml propidium iodide (PI) and 500 µg/mL
665 RNAse (Sigma-Aldrich). FACS data were obtained using FacsCalibur BD flow
666 cytometer and visualized using Flowing software (http://www.flowingsoftware.com/ -
667 versions 2.4.1 and above).

668

669 **Subcellular fractionation and immunoblotting**

670 Chromatin and nucleoplasmic fractions were prepared from cell pellets essentially as
671 described and protein concentrations were determined with the BCA method
672 (Pierce). For immunoblotting, 10 µg of chromatin and 15 µg of soluble nuclear
673 material were loaded on 10% or 12% polyacrylamide gels and transferred onto PVDF
674 membranes. After blocking with 2% BSA, the corresponding antibodies were
675 incubated for 14-16 h at 4°C.

676

677 **Mass spectrometry**

678 Protein samples containing the nucleoskeleton and chromatin were resuspended in
679 2x Laemmli buffer and sonicated. Proteins (corresponding to 0.5 ml of extract) were
680 reduced, alkylated and separated by SDS-PAGE in 4-20% gradient gels (Bio-Rad),
681 each lane was sliced in 15 pieces and in-gel trypsin (Gold, Promega) digestion, and
682 peptide extraction were performed essentially as described (Shevchenko *et al*, 2006).
683 Obtained peptides were analyzed online by nano-flow HPLC-nanoelectrospray
684 ionization using a LTQ Orbitrap XL mass spectrometer (Thermo Fisher Scientific)

685 coupled to an Ultimate 3000 HPLC (Dionex, Thermo Fisher Scientific). Desalting and
686 pre-concentration of samples were performed online on a Pepmap® pre-column (0.3
687 mm x 10 mm, Dionex). A gradient consisting of 0-40% B in A for 60 min, followed by
688 80% B/20% A for 15 min (A = 0.1% formic acid, 2% acetonitrile in water; B = 0.1 %
689 formic acid in acetonitrile) at 300 nL/min was used to elute peptides from the capillary
690 reverse- phase column (0.075 mm x 150 mm, Pepmap®, Dionex). Eluted peptides
691 were electrosprayed online at a voltage of 2.2 kV. A cycle of one full-scan mass
692 spectrum (400 – 2,000 m/z) at a resolution of 60,000 (at 400 m/z), followed by 5
693 data-dependent MS/MS spectra was repeated continuously throughout the nanoLC
694 separation. All MS/MS spectra were recorded using normalised collision energy (35
695 %, activation Q 0.25 and activation time 30 ms) with an isolation window of 3 m/z.
696 Raw data analysis was performed using the MaxQuant software (v. 1.3.0.5). Peak
697 lists were searched against the NCBI *Xenopus laevis* (release 130117;
698 http://www.ncbi.nlm.nih.gov), 255 frequently observed contaminants as well as
699 reversed sequences of all entries. The *X. laevis* genome is not fully sequenced and
700 this results in several 'uncharacterized proteins'. Therefore, we also searched against
701 the *X. tropicalis* database, which is fully sequenced. The following settings were
702 applied: spectra were searched with a mass tolerance of 7 ppm (MS) and 0.5 m/z
703 (MS/MS). Enzyme specificity was set to Trypsin/P. Up to two missed cleavages were
704 allowed and only peptides with at least six amino acids in length were considered.
705 Carbamidomethylation of Cys was selected as fixed modification. Oxidation on
706 methionine, phosphorylation on serine, threonine or tyrosine and acetylation on
707 Protein N-term was set as a variable modification. Peptide identifications were
708 accepted based on their false discovery rate (< 1%). Accepted peptide sequences
709 were subsequently assembled by MaxQuant into proteins to achieve a false

discovery rate of 1% at the protein level. Only proteins identified by at least 1 unique peptide or 2 peptides of at least 6 amino acids and in at least 2 of the 3 replicates were selected for further analyses.

For quantitation, the log10 of median intensity-based absolute quantification (iBAQ) was used. To compensate for the incomplete *X. laevis* database, MaxQuant .txt files were modified as follows: matchgroups were created with protein groups identified by similar peptides; GO categories for identified *X. laevis* proteins were downloaded from Uniprot after converting the GI IDs into UniprotKB accession numbers and added manually in the MaxQuant files before being loaded onto Perseus; information on "uncharacterized proteins" was extracted by assigning the UniRef90 or Uniref50 cluster. In Perseus, two groups were defined: "IBAQ D" for DMSO (control), "IBAQ P" for purvalanol A-treated (CDK-inhibited) sample. "NaN values" were converted to "0", so that proteins identified in only one of the 2 conditions would be included in the plots. Statistical analysis was performed in Perseus selecting the 2-sample t-test with Benjamini-Hochberg and FDR 1% as parameters.

For Gene Ontology analysis in DAVID (Huang da *et al*, 2009), gene names were loaded using *Xenopus laevis* as background. All terms are presented in EV Tables but only GO BP with p-value <0.01 were further analyzed in REVIGO to remove redundant GO terms (for Figure 1B) with the following settings: SimRel method, whole Uniprot database (default settings) and Small Similarity (0.5).

Acknowledgements

This work was supported by ANR grant ANR-09-BLAN-0252 and Ligue Nationale Contre le Cancer, ''Equipe labellisée,'' grants EL2010. LNCC/DF and EL2013. LNCC/DF and the Région Languedoc Roussillon. Thanks to the labs of J. Blow, M.

Méchali, D. Görlich, B. Huelsmann, D. Maiorano and M. Hahne for providing antibodies, R. Grosse for the Lifeact-GFP-NLS, the actin-NLS R62D and all formin vectors. Thanks to B.C. Lee and V. Gladyshev for MICAL reagents. H. Hochegger, I. Hagan, P. Jay, V. Dulic, J. Hutchins and A. Crevenna for comments on the manuscript. Thanks to M. Goldberg for advice on sample preparation for electron microscopy, C. Cazevieille of the CRIC-IURS, D. Cot of the IEM, V. Georget, J. M. Langerak and J. Cau of MRI imaging facilities, Montpellier, for assistance with electron and light microscopy and analysis. Thanks to R. Audo for help with NF-κB experiments.

Author Contributions

NP and LK conceived, performed and analysed most experiments and wrote the manuscript. BH performed other experiments. SU and NP performed proteomics. MR co-supervised NP for proteomics. AC provided an important intellectual contribution. JD supervised NPE experiments. NM co-supervised nuclear transport experiments. DF conceived and directed the study and wrote the manuscript.

Conflict of Interest Statement

The authors declare no competing interests.

Supplementary information.

Supplementary information includes 6 videos and 4 tables.

References

757 Allen TD, Rutherford SA, Murray S, Gardiner F, Kiseleva E, Goldberg MW &
758 Drummond SP (2007) Visualization of the nucleus and nuclear envelope in
759 situ by SEM in tissue culture cells. *Nat. Protoc.* **2:** 1180–1184
760 Arias EE & Walter JC (2004) Initiation of DNA replication in Xenopus egg extracts.
761 *Front. Biosci. J. Virtual Libr.* **9:** 3029–45
762 Assoian RK & Zhu X (1997) Cell anchorage and the cytoskeleton as partners in
763 growth factor dependent cell cycle progression. *Curr. Opin. Cell Biol.* **9:** 93–8
764 Baarlink C, Wang H & Grosse R (2013) Nuclear actin network assembly by formins
765 regulates the SRF coactivator MAL. *Science* **340:** 864–7
766 Bai L, Michael WM & Yan S (2014) Importin β-dependent nuclear import of TopBP1
767 in ATR-Chk1 checkpoint in Xenopus egg extracts. *Cell. Signal.* **26:** 857–867
768 Blow JJ & Laskey RA (1986) Initiation of DNA replication in nuclei and purified DNA
769 by a cell-free extract of Xenopus eggs. *Cell* **47:** 577–87
770 Bompard G, Rabeharivelo G, Frank M, Cau J, Delsert C & Morin N (2010) Subgroup
771 II PAK-mediated phosphorylation regulates Ran activity during mitosis. *J. Cell*
772 *Biol.* **190:** 807–822
773 Burgess A, Lorca T & Castro A (2012) Quantitative live imaging of endogenous DNA
774 replication in mammalian cells. *PloS One* **7:** e45726
775 Clark TG & Rosenbaum JL (1979) An actin filament matrix in hand-isolated nuclei of
776 X. laevis oocytes. *Cell* **18:** 1101–1108
777 Densham RM, O'Neill E, Munro J, König I, Anderson K, Kolch W & Olson MF (2009)
778 MST kinases monitor actin cytoskeletal integrity and signal via c-Jun N-
779 terminal kinase stress-activated kinase to regulate p21Waf1/Cip1 stability.
780 *Mol. Cell. Biol.* **29:** 6380–6390

781 Dopie J, Rajakylä EK, Joensuu MS, Huet G, Ferrantelli E, Xie T, Jäälinoja H, Jokitalo
782 E & Vartiainen MK (2015) Genome-wide RNAi screen for nuclear actin reveals
783 a network of cofilin regulators. *J. Cell Sci.*
784 Dopie J, Skarp K-P, Rajakylä EK, Tanhuanpää K & Vartiainen MK (2012) Active
785 maintenance of nuclear actin by importin 9 supports transcription. *Proc. Natl.*
786 *Acad. Sci. U. S. A.* **109:** E544-552
787 Echalier A, Cot E, Camasses A, Hodimont E, Hoh F, Jay P, Sheinerman FB,
788 Krasinska L & Fisher D (2012) An integrated chemical biology approach
789 provides insight into Cdk2 functional redundancy and inhibitor sensitivity.
790 *Chem Biol* **19:** 1028–1040
791 Feric M & Brangwynne CP (2013) A nuclear F-actin scaffold stabilizes
792 ribonucleoprotein droplets against gravity in large cells. *Nat. Cell Biol.* **15:**
793 1253–1259
794 Gauvin TJ, Fukui J, Peterson JR & Higgs HN (2009) Isoform-selective chemical
795 inhibition of mDia-mediated actin assembly. *Biochemistry (Mosc.)* **48:** 9327–
796 9329
797 Gounon P & Karsenti E (1981) Involvement of contractile proteins in the changes in
798 consistency of oocyte nucleoplasm of the newt Pleurodeles waltlii. *J. Cell Biol.*
799 **88:** 410–421
800 Grosse R & Vartiainen MK (2013) To be or not to be assembled: progressing into
801 nuclear actin filaments. *Nat. Rev. Mol. Cell Biol.* **14:** 693–7
802 Hetzer MW, Walther TC & Mattaj IW (2005) Pushing the envelope: structure,
803 function, and dynamics of the nuclear periphery. *Annu. Rev. Cell Dev. Biol.*
804 **21:** 347–80

805 Hofmann WA, Stojiljkovic L, Fuchsova B, Vargas GM, Mavrommatis E, Philimonenko
806 V, Kysela K, Goodrich JA, Lessard JL, Hope TJ, Hozak P & de Lanerolle P
807 (2004) Actin is part of pre-initiation complexes and is necessary for
808 transcription by RNA polymerase II. *Nat. Cell Biol.* **6:** 1094–1101
809 Hu P, Wu S & Hernandez N (2004) A role for beta-actin in RNA polymerase III
810 transcription. *Genes Dev.* **18:** 3010–3015
811 Huang da W, Sherman BT & Lempicki RA (2009) Systematic and integrative analysis
812 of large gene lists using DAVID bioinformatics resources. *Nat. Protoc.* **4:** 44–
813 57
814 Huang W, Ghisletti S, Saijo K, Gandhi M, Aouadi M, Tesz GJ, Zhang DX, Yao J,
815 Czech MP, Goode BL, Rosenfeld MG & Glass CK (2011) Coronin 2A
816 mediates actin-dependent de-repression of inflammatory response genes.
817 *Nature* **470:** 414–418
818 Huet G, Skarp K-P & Vartiainen MK (2012) Nuclear actin levels as an important
819 transcriptional switch. *Transcription* **3:** 226–230
820 Iida K, Iida H & Yahara I (1986) Heat shock induction of intranuclear actin rods in
821 cultured mammalian cells. *Exp. Cell Res.* **165:** 207–215
822 Johnson MA, Sharma M, Mok MTS & Henderson BR (2013) Stimulation of in vivo
823 nuclear transport dynamics of actin and its co-factors IQGAP1 and Rac1 in
824 response to DNA replication stress. *Biochim. Biophys. Acta* **1833:** 2334–2347
825 Kalendová A, Kalasová I, Yamazaki S, Uličná L, Harata M & Hozák P (2014) Nuclear
826 actin filaments recruit cofilin and actin-related protein 3, and their formation is
827 connected with a mitotic block. *Histochem. Cell Biol.* **142:** 139–152

828 Kapoor P, Chen M, Winkler DD, Luger K & Shen X (2013) Evidence for monomeric
829 actin function in INO80 chromatin remodeling. *Nat. Struct. Mol. Biol.* **20:** 426–
830 432
831 Khoudoli GA, Gillespie PJ, Stewart G, Andersen JS, Swedlow JR & Blow JJ (2008)
832 Temporal Profiling of the Chromatin Proteome Reveals System-wide
833 Responses to Replication Inhibition. *Curr Biol* **18:** 838–43
834 Krauss SW, Chen C, Penman S & Heald R (2003) Nuclear actin and protein 4.1:
835 essential interactions during nuclear assembly in vitro. *Proc Natl Acad Sci U A*
836 **100:** 10752–7
837 Lanerolle P de (2012) Nuclear actin and myosins at a glance. *J Cell Sci* **125:** 4945–
838 4949
839 Lee SJ, Matsuura Y, Liu SM & Stewart M (2005) Structural basis for nuclear import
840 complex dissociation by RanGTP. *Nature* **435:** 693–696
841 Lowe AR, Siegel JJ, Kalab P, Siu M, Weis K & Liphardt JT (2010) Selectivity
842 mechanism of the nuclear pore complex characterized by single cargo
843 tracking. *Nature* **467:** 600–603
844 Lundquist MR, Storaska AJ, Liu TC, Larsen SD, Evans T, Neubig RR & Jaffrey SR
845 (2014) Redox modification of nuclear actin by MICAL-2 regulates SRF
846 signaling. *Cell* **156:** 563–76
847 Martinez Molina D, Jafari R, Ignatushchenko M, Seki T, Larsson EA, Dan C,
848 Sreekumar L, Cao Y & Nordlund P (2013) Monitoring drug target engagement
849 in cells and tissues using the cellular thermal shift assay. *Science* **341:** 84–87
850 McDonald D, Carrero G, Andrin C, de Vries G & Hendzel MJ (2006) Nucleoplasmic
851 beta-actin exists in a dynamic equilibrium between low-mobility polymeric
852 species and rapidly diffusing populations. *J. Cell Biol.* **172:** 541–552

853 Miyamoto K, Pasque V, Jullien J & Gurdon JB (2011) Nuclear actin polymerization is
854 required for transcriptional reprogramming of Oct4 by oocytes. *Genes Dev.*
855 **25:** 946–958
856 Miyamoto K, Teperek M, Yusa K, Allen GE, Bradshaw CR & Gurdon JB (2013a)
857 Nuclear Wave1 Is Required for Reprogramming Transcription in Oocytes and
858 for Normal Development. *Science* **341:** 1002–1005
859 Miyamoto K, Teperek M, Yusa K, Allen GE, Bradshaw CR & Gurdon JB (2013b)
860 Nuclear Wave1 is required for reprogramming transcription in oocytes and for
861 normal development. *Science* **341:** 1002–1005
862 Mohr D, Frey S, Fischer T, Güttler T & Görlich D (2009) Characterisation of the
863 passive permeability barrier of nuclear pore complexes. *EMBO J.* **28:** 2541–
864 2553
865 Morel J, Audo R, Hahne M & Combe B (2005) Tumor necrosis factor-related
866 apoptosis-inducing ligand (TRAIL) induces rheumatoid arthritis synovial
867 fibroblast proliferation through mitogen-activated protein kinases and
868 phosphatidylinositol 3-kinase/Akt. *J. Biol. Chem.* **280:** 15709–15718
869 Németh ZH, Deitch EA, Davidson MT, Szabó C, Vizi ES & Haskó G (2004)
870 Disruption of the actin cytoskeleton results in nuclear factor-kappaB activation
871 and inflammatory mediator production in cultured human intestinal epithelial
872 cells. *J. Cell. Physiol.* **200:** 71–81
873 Nolen BJ, Tomasevic N, Russell A, Pierce DW, Jia Z, McCormick CD, Hartman J,
874 Sakowicz R & Pollard TD (2009) Characterization of two classes of small
875 molecule inhibitors of Arp2/3 complex. *Nature* **460:** 1031–4
876 Obrdlik A & Percipalle P (2011) The F-actin severing protein cofilin-1 is required for
877 RNA polymerase II transcription elongation. *Nucl. Austin Tex* **2:** 72–79

878 Philimonenko VV, Zhao J, Iben S, Dingová H, Kyselá K, Kahle M, Zentgraf H,
879 Hofmann WA, de Lanerolle P, Hozák P & Grummt I (2004) Nuclear actin and
880 myosin I are required for RNA polymerase I transcription. *Nat. Cell Biol.* **6:**
881 1165–1172
882 Plessner M, Melak M, Chinchilla P, Baarlink C & Grosse R (2015) Nuclear F-actin
883 Formation and Reorganization upon Cell Spreading. *J. Biol. Chem.* **290:**
884 11209–11216
885 Poulet A, Arganda-Carreras I, Legland D, Probst AV, Andrey P & Tatout C (2015)
886 NucleusJ: an ImageJ plugin for quantifying 3D images of interphase nuclei.
887 *Bioinforma. Oxf. Engl.* **31:** 1144–1146
888 Rando OJ, Zhao K, Janmey P & Crabtree GR (2002) Phosphatidylinositol-dependent
889 actin filament binding by the SWI/SNF-like BAF chromatin remodeling
890 complex. *Proc Natl Acad Sci U A* **99:** 2824–9
891 Rizvi SA, Neidt EM, Cui J, Feiger Z, Skau CT, Gardel ML, Kozmin SA & Kovar DR
892 (2009) Identification and characterization of a small molecule inhibitor of
893 formin-mediated actin assembly. *Chem. Biol.* **16:** 1158–68
894 Rosenblatt J, Cramer LP, Baum B & McGee KM (2004) Myosin II-dependent cortical
895 movement is required for centrosome separation and positioning during mitotic
896 spindle assembly. *Cell* **117:** 361–372
897 Sanger JW, Sanger JM, Kreis TE & Jockusch BM (1980) Reversible translocation of
898 cytoplasmic actin into the nucleus caused by dimethyl sulfoxide. *Proc. Natl.*
899 *Acad. Sci. U. S. A.* **77:** 5268–5272
900 Schindelin J, Arganda-Carreras I, Frise E, Kaynig V, Longair M, Pietzsch T, Preibisch
901 S, Rueden C, Saalfeld S, Schmid B, Tinevez J-Y, White DJ, Hartenstein V,

902 Eliceiri K, Tomancak P & Cardona A (2012) Fiji: an open-source platform for
903 biological-image analysis. *Nat. Methods* **9:** 676–682
904 Schliwa M (1982) Action of cytochalasin D on cytoskeletal networks. *J. Cell Biol.* **92:**
905 79–91
906 Schroeder TE (1973) Actin in dividing cells: contractile ring filaments bind heavy
907 meromyosin. *Proc. Natl. Acad. Sci. U. S. A.* **70:** 1688–1692
908 Serebryannyy LA, Parilla M, Annibale P, Cruz CM, Laster K, Gratton E, Kudryashov
909 D, Kosak ST, Gottardi CJ & de Lanerolle P (2016) Persistent nuclear actin
910 filaments inhibit transcription by RNA polymerase II. *J. Cell Sci.*
911 Sero JE, Sailem HZ, Ardy RC, Almuttaqi H, Zhang T & Bakal C (2015) Cell shape
912 and the microenvironment regulate nuclear translocation of NF-κB in breast
913 epithelial and tumor cells. *Mol. Syst. Biol.* **11:** 790
914 Shevchenko A, Tomas H, Havlis J, Olsen JV & Mann M (2006) In-gel digestion for
915 mass spectrometric characterization of proteins and proteomes. *Nat Protoc* **1:**
916 2856–60
917 Small J, Rottner K, Hahne P & Anderson KI (1999) Visualising the actin cytoskeleton.
918 *Microsc. Res. Tech.* **47:** 3–17
919 Soderholm JF, Bird SL, Kalab P, Sampathkumar Y, Hasegawa K, Uehara-Bingen M,
920 Weis K & Heald R (2011) Importazole, a small molecule inhibitor of the
921 transport receptor importin-beta. *ACS Chem. Biol.* **6:** 700–8
922 Spencer VA, Costes S, Inman JL, Xu R, Chen J, Hendzel MJ & Bissell MJ (2011)
923 Depletion of nuclear actin is a key mediator of quiescence in epithelial cells. *J.*
924 *Cell Sci.* **124:** 123–132
925 Stüven T, Hartmann E & Görlich D (2003) Exportin 6: a novel nuclear export receptor
926 that is specific for profilin.actin complexes. *EMBO J.* **22:** 5928–5940

927 Uzbekov R, Kireyev I & Prigent C (2002) Centrosome separation: respective role of
928 microtubules and actin filaments. *Biol. Cell Auspices Eur. Cell Biol. Organ.* **94:**
929 275–288
930 Vartiainen MK, Guettler S, Larijani B & Treisman R (2007) Nuclear actin regulates
931 dynamic subcellular localization and activity of the SRF cofactor MAL. *Science*
932 **316:** 1749–52
933 Walter J, Sun L & Newport J (1998) Regulated chromosomal DNA replication in the
934 absence of a nucleus. *Mol Cell* **1:** 519–29
935 Wu X, Yoo Y, Okuhama NN, Tucker PW, Liu G & Guan J-L (2006) Regulation of
936 RNA-polymerase-II-dependent transcription by N-WASP and its nuclear-
937 binding partners. *Nat. Cell Biol.* **8:** 756–763
938 Yoo Y, Wu X & Guan J-L (2007) A novel role of the actin-nucleating Arp2/3 complex
939 in the regulation of RNA polymerase II-dependent transcription. *J. Biol. Chem.*
940 **282:** 7616–7623
941

942 **Figure Legends**

943 **Figure 1 - The proteome of replicating nuclei.**

944 **A** Replication time-course of sperm chromatin in control and Purvalanol A (PA)-
945 treated egg extracts, with nuclei isolated for MS analysis at 50 min.

946 **B** Graphical representation of the identified proteome with relative quantitation data
947 (mean values from 3 replicates). Full dataset, Table S1.

948 **C** Volcano plot combining the fold-change between control and CDK-inhibited
949 conditions with their log10 *P*-values (Student's t-test). The most significantly
950 differentially abundant proteins are highlighted.

951 **D** GO analysis using DAVID, showing the most highly enriched GO biological
952 processes in each condition (full GO analysis, Table S2). NE: not enriched.
953 **E** Western blots of chromatin fractions from control and PA-treated nuclei used for
954 MS analysis.
955
956 **Figure 2 - Nuclear actin dynamics during the cell cycle.**
957 **A** Immunofluoresence images of the actin regulators indicated, analysed 60 min after
958 sperm head addition. Bar, 10µm.
959 **B** Western blot analysis of cytoplasm (CP), whole nuclear (NC), nucleoplasmic (NP)
960 and insoluble (P) fraction at 60min-time point during DNA replication, probed with
961 antibodies against proteins indicated.
962 **C** Actin filaments formed by actin-Alexa Fluor 488 in XEE, counterstained with
963 phalloidin. Bar, 10µm.
964 **D** Immunofluorescence image of nucleus incubated in control extract for 60min in the
965 presence of actin-Alexa Fluor488. Bar, 10 µm.
966 **E** Deconvolved images of 3D optical sections of a nucleus. Left panel, surface; right
967 panel, mid-section. Actin (actin-biotin; red), DNA (blue), NUPs (mAb414, green). Bar,
968 5µm.
969 **F** Immunofluorescence images of nucleus formed in control extract, stained at 60 min
970 with DNaseI-Alexa Fluor 594. Bar, 10µm.
971 **G** Early G1 U2OS cells expressing actin-NLS chromobody co-stained with phalloidin
972 and DAPI (DNA). Bar, 5µm.
973 **H** Duration of early G1 nuclear actin network (mean ± SD, n=135 cells from 3
974 independent experiments).

I Serial confocal planes of an early G1 U2OS cell fixed with glutaraldehyde and stained with phalloidin and DAPI. Bar, 5µm.

Figure 3 - Effect of actin drugs, regulators and probes on nuclear actin dynamics and abundance in *Xenopus* egg extracts.

A Nuclei were allowed to form for 30 min before drugs (Cyt D, CD; SMIFH2, SF; latrunculin A, LA; jasplakinolide, Jpk; Cyt D and latrunculin A, CD+LA; SMIFH2 and latrunculin A, SF+LA) or Arp2/3 recombinant protein (in combination with VCA domain of WASP) were added, then purified at 45 min. Soluble and insoluble nuclear fractions were blotted for actin.

B Extract was supplemented with sperm nuclei and actin-Alexa Fluor 488; at 40 min indicated drugs or Arp2/3 and VCA domain of WASP were added, and nuclei were analysed for fluorescent actin at 55 min. Long exposure time (2000ms) was needed to visualise nuclear actin in all conditions with the exception of Cyt D and jasplakinolide (exposure time 200ms, highlighted in red). Bar, 10µm.

C Extract was supplemented with sperm nuclei; at 45 min Cyt D (CD) was added and nuclei were analysed at 60 min and stained with phalloidin. Bar, 10µm.

Figure 4 - DNA replication requires actin dynamics.

A FACS analysis of U2OS cells synchronised in G1 and treated with DMSO (Ctl) or SMIFH2 (50µM).

B Immunofluorescent images of control or SMIFH2-treated (1hr pre-treatment, 1hr co-incubation) U2OS cells pulsed for 1hr with EU. Bar, 5µm.

C Quantification of EU incorporation (1hr) in U2OS cells, control or transfected with mDia2 DAD.NLS or DAD constructs (n>100, 61 and 47, respectively).

D Quantification of EdU incorporation from 2 independent experiments after a 60 min-pulse in U2OS cells expressing formin constructs (left) or actin-NLS mutants (right) (**, *p*-value<0.001, ***, *p*-value<0.0001; Student's *t*-test).

E Quantification (mean ± SEM) of EdU intensity from **D** normalised to the non-transfected cells.

F Duration of PCNA foci in U2OS cells expressing PCNA chromobody (each dot represents the mean of 5-7 foci per cell, mean ± SD of 29 and 11 cells, respectively, per condition from 2 independent experiments).

G Chromosomal DNA replication determined by ^{33}P-dCTP incorporation assay in control conditions or with Cyt D (CD); mean ± SEM of 8 independent experiments.

H DNA replication assessed in control extract, or extracts supplemented with CytD D (CD), with or without latrunculin A (LA). A representative experiment of 5 independent experiments is shown.

I DNA replication assays in control (Ctl) or formin-inhibited (SMIFH2; 500µM) extract; mean ± SEM of 8 independent experiments.

J Chromatin loading of pre-RC and pre-IC factors in control conditions (Ctl) or with Cyt D (CD).

Figure 5 - NPC formation requires actin dynamics.

A Immunofluorescence images of nuclei formed either in control extracts or in the presence of indicated drugs or MICAL2, analysed at 60 min. Bar, 10µm.

B Left, confocal planes of nuclei of cells treated with DMSO (Ctl) or SMIFH2 (50µM) for 4 h, stained with mAb414 and DAPI (DNA). Bar, 5µm. Right, characterisation of nuclear morphology (mean ± SD of 20 cells from 2 independent experiments; ***, *p*-value <0.0001, Student's *t*-test).

C 3D-SIM images of the nuclear lamina (red), NUPs (mAb414, green), in control or formin-inhibited (SMIFH2) conditions. A reconstructed 3D image (top) and a section (bottom) of the same nucleus are shown. In sections, DNA is shown (blue). Bar, 5µm.
D Scanning electron microscopy (FEISEM) images of nuclei formed in the presence of DMSO (Ctl), Cyt D or SMIFH2 at 50min. Representative NPCs (yellow arrowheads) or incompletely formed NPCs (white arrowheads). Magnification x40,000. Bar, 100nm.

Figure 6 - Nuclear transport requires actin dynamics.

A Immunofluorescence images of nuclei formed in control or Cyt D (CD)- or SMIFH2-treated extracts. Nuclear membranes were visualised with the lipid dye DHCC; nuclear transport was assayed with NLS-tagged GST-GFP protein added at the onset of experiment. Nuclei were analysed at 60 min. Bar, 10µm.
B Top, scheme: nuclei were supplemented which Cyt D (CD), SMIFH2, PA, WGA or importazole (Imp) at 50 min; NLS-GST-GFP was added at 60 min and nuclei were imaged at 75 min. Bar, 10µm.
C Immunofluorescence images of RA-FLS fibroblasts, treated for one hour with DMSO (Ctl), Importazole (50µM), Cyt D (40µM), or SMIFH2 (50µM), subsequently stimulated or not with IL-1β or TNF-α, stained for NFκB. Bar, 20µm.
D Quantification of the data presented in **C**. Mean nuclear/cytoplasmic NFκB intensity ratio (±SD) of two independent experiments using two different fibroblast sources; n≥400 for each condition; CytD sample was lost in exp 2.

Figure 7 - Disruption of actin dynamics hinders cargo release from importin.

A Scheme: control extract (Ctl) or extract treated with Cyt D (CD) or importazole (Imp) was incubated for 30 min and immunoprecipitated with mAb414 (Mock IP, no antibody added). Beads were blotted for the proteins indicated.

B Scheme: nuclei, formed in control extract, or with Cyt D (CD) added at 45 min, were purified at 60 min and mAb414 used for immunoprecipitation; 10% of lysed nuclei was used as input. Beads were blotted with the proteins indicated.

C Scheme: nuclei were incubated in extract supplemented at 45 min with Cyt D (CD) or SMIFH2, lysed and pulled-down with GST-Ran WT immobilised on glutathione beads, or control beads (Mock). Beads were blotted with the proteins indicated.

D *In vitro* pull-down using GST or GST-RanWT immobilised on glutathione beads and actin-biotin; beads were blotted for actin and Ran.

E *In vitro* pull-down between actin-biotin and glutathione-immobilized GST or GST-Ran WT, pre-loaded with either GTP or GDP; beads were blotted for actin or GST.

F Scheme: nuclei, formed in control extract, supplemented at 45 min with RanQ69L, Cyt D (CD) or SMIFH2 (FH), without or with latrunculin A (LA), were lysed and immunoprecipitated with anti-active Ran antibodies (Mock IP, no antibody added). Beads were blotted for actin and Ran.

Figure 8 - Formins promote pre-IC formation in parallel with CDK.

A Scheme: nuclei were formed in the first extract containing geminin, then transferred to a second extract, with Cdt1, which was either Mock- (MockΔ) or WGA-binding protein- (WGA-bpΔ) depleted, with or without addition of SMIFH2; or where WGA was added (+WGA). Replication efficiency was measured in the second extract.

B Scheme: double reciprocal nuclear transfer, from geminin-treated extract into either SMIFH2- or WGA-treated Cdt1-containing extract, with aphidicolin; and then into a third extract with the alternative condition. DNA replication was assessed in the third extract.

C Scheme: nuclear transfer experiment, in which first extracts contained geminin; second extracts contained Cdt1 and were controls (Ctl), or CDKs (PA) or formins (SMIFH2) were inhibited. DNA replication was assessed in the second extract.

D Chromatin was purified from second extracts of experiment in **c** and blotted for the proteins indicated. LC, loading control.

E Scheme: reciprocal nuclear transfer experiment, in which first extracts contained aphidicolin (Aphi) and either PA or SMIFH2 or were controls; nuclei were isolated from each extract after 45 min and transferred to the same combination of conditions. DNA replication was assessed in the second extract.

Figure 9 - Nuclear formin activity controls chromatin loading of PCNA and CDKs.

A-C Scheme: nuclear transfer from the first extract, where active nuclear export (Leptomycin B, LB) and CDK (PA) were inhibited, into the second extract, either control or treated with SMIFH2, containing leptomycin B or not.

B DNA replication was assessed in the second extract.

C Total nuclear and chromatin-associated replication factors in nuclei isolated at 60 min were analysed by Western blotting.

D Chromosomal DNA replication in NPE determined by ^{33}P-dCTP incorporation assay in control conditions (Ctl) or in the presence of SMIFH2; mean ± SEM of 4 independent experiments.

E Chromatin loading at 30 min of indicated replication factors in NPE, in control (Ctl) or SMIFH2-treated extracts.

Supplementary Figure legends

Supplementary Figure 1 - Scatter plots showing the high reproducibility of MS/MS runs between replicates.

Supplementary Figure 2 - Effect of actin drugs and probes on nuclear actin dynamics and form in human cells.

A U2OS cells transiently expressing Lifeact-NLS-GFP, fixed and stained with phalloidin and DAPI (DNA). Bar, 5 µm.

B Interphase U2OS cells expressing actin-NLS chromobody co-stained with mAb414 antibody and DAPI treated with DMSO (Ctl) or SMIFH2 (50 µM) for 2 hours. Bar, 5µm.

C Snapshots of live U2OS cells expressing actin-NLS chromobody or Lifeact-GFP-NLS in the presence of DMSO (Ctl) or SMIFH2 (50µM). Numbers represent the percent of cells showing the presented phenotype; n>100 cells in each condition from ≥3 independent experiments. Bar, 5µm.

Supplementary Figure 3 - Disrupting actin dynamics hinders DNA replication and causes replication stress in human cells.

A FACS analysis of G1-synchronised U2OS cells in the presence of increasing concentrations of SMIFH2. Cells were collected when control cells were in S-phase (+14h).

B FACS analysis of HeLa cells, synchronised in G1 as in Fig 4A, and treated with DMSO (Ctl) or SMIFH2, collected at the time points indicated.

C Immunoblotting of chromatin and nucleoplasmic fractions from cells in Fig 4A. FACS profiles for each time-point are shown. Ctl, U2OS cell lysate; LC, loading control.

D Quantification of EU signal intensity from experiment presented in Fig. 2b (n>400).

E Immunofluorescence images of U2OS cells transfected with the indicated FLAG-tagged actin-NLS constructs. DNA was stained with DAPI, actin-NLS constructs with anti-Flag antibody. Bar, 5μm.

F Asynchronous (AS) or double-thymidine block (DTB) S-phase-synchronised U2OS cells were treated for 2hrs with DMSO, bleomycin (Bleo), or SMIFH2, and stained for γH2A.X. Corresponding FACS profiles are shown.

G Quantification of γH2A.X-positive cell number from experiment presented in F, and in cells transiently transfected with mDia2 DAD.NLS or DAD constructs. Cells with >10 foci were considered positive.

Supplementary Figure 4 - Effect of actin drugs and actin regulators on DNA replication in *Xenopus* egg extracts.

A Replication time-course of sperm chromatin in extract treated with Cyt D (CD), gelsolin, Cyt D and gelsolin (CD+Gel), jasplakinolide (Jspk), or Cyt D and jasplakinolide (CD+Jspk).

B-E Replication assays in control extract or in extracts supplemented with Cyt D (CD) with or without cofilin (**B**); recombinant MICAL2 protein (**C**), formin inhibitor 2.4 (**D**), or Arp2/3 inhibitor CK666 or its inactive analogue CK689 (**E**).

F Chromatin loading of pre-RC and pre-IC factors in control conditions or in the presence of SMIFH2 (500µM). LC, loading control.

G, H Interaction of endogenous proteins indicated and biotin-dUTP was probed by PLA in nuclei formed in control XEE for 60 min. Primary anti-actin rabbit antibodies were combined with secondary rabbit PLA probes. Bar, 10µm.

I Nuclei formed in control extract, were lysed at 60 min and actin was precipitated using biotinylated Lifeact peptide immobilised on streptavidin beads (Mock IP, no peptide); beads were blotted for actin and PCNA.

Supplementary Figure 5 - Active nuclear transport requires actin dynamics.

A Western blots of total nuclear fractions in control and formin-inhibited (SMIFH2) extracts, probed with antibodies to the NUPs indicated; the same number of nuclei was analysed for each condition.

B Scheme: Nuclei were formed in control extract or in the presence of Cyt D (CD), SMIFH2, WGA or Triton; at 35 min. Dextran10-Alexa488 (Dex10-A488) or Dextran70-rhodamine (Dex70-rhod) were added; nuclei were imaged directly at 50 min. Bar, 10µm.

C Immunofluorescence images of nuclei formed for 5 and 15 min in control or cytochalasin D-treated extracts, stained for DNA, Elys, RCC1, importin-β and FG-NUPs (mAb414). Bar, 10µm.

D Replication time course of sperm chromatin in extract treated with importazole (Imp) at the concentrations indicated.

E Scheme: Nuclei were formed in control extract; at 45 min Cyt D (CD), SMIFH2, WGA or Triton were added, followed by addition of Dextran10-Alexa488 (Dex10-

A488) or Dextran70-rhodamine (Dex70-rhod); nuclei were imaged directly at 75 min. Bar, 10µm.

Supplementary Figure 6 - Ongoing nuclear transport is required to promote DNA replication.

A Replication assay in control extract and in extract supplemented with WGA at the concentrations indicated (mg/ml).

B Replication assay of Mock- and WGA-binding protein-depleted (WGA-bpΔ) extract.

C Left, immunofluorescence images of nuclei formed for 60 min in control and geminin(40nM)-containing extracts, stained for DNA, NUPs (mAb414) and Lamin B3. Bar, 10µm. Right, replication time-course of control and geminin-treated extract.

D Scheme: reciprocal nuclear transfer experiment, in which first extracts contained aphidicolin (Aphi) and either PA or WGA, or were control; nuclei were isolated after 45 min and transferred to the alternative condition; DNA replication was assayed in the second extract.

E Replication time course of sperm chromatin in NPE extract treated with SMIFH2 or 2.4 formin inhibitor (mean values of two replicates), both used at 200µM.

F Western blot for indicated proteins of chromatin fractions with or without addition of NPE.

Table S1: Entire MS/MS Dataset. Proteins identified in the nuclear structural proteome of control and CDK-inhibited extracts.

Table S2: GO Annotations of the nuclear structural proteome using DAVID.

1196 **Table S3: Actin regulators identified in the structure proteome of nuclei**

1197

Protein or gene name	Log_{10} Mean iBAQ values	
	Ctl	PA (CDK-inhib)
actin-related protein 2-A	8.72	8.84
Actin-related protein 2/3 complex subunit 4	8.56	8.73
ARP3 actin-related protein 3	8.51	8.70
capping protein muscle Z-line. beta – capzb	8.33	8.54
capping protein muscle Z-line. alpha 2	8.12	8.33
Actin-related protein 2/3 complex subunit 2	8.11	8.37
ISWI protein	7.97	8.01
Actin-related protein 2/3 complex subunit 3	7.8	8.04
Actin-related protein 2/3 complex subunit 1A	7.63	7.76
LIM domain and actin binding 1	7.60	7.70
Coronin 1C	7.53	7.64
actinin alpha 4	7.52	7.70
F-actin-capping protein subunit alpha-1	7.51	7.75
actin-like 6A	7.51	7.44
ARP1 actin-related protein 1 homolog A	7.49	7.44
Smarcc1 protein	7.49	7.38
Cortactin – Cttn	7.43	7.53
Actin-related protein 2/3 complex subunit 5	7.42	7.70
SWI/SNF-related matrix-associated actin-dependent regulator of chromatin subfamily B member 1	7.41	7.38
Cofilin 1A	7.15	7.44

Smarce1	7.14	7.16
Smarcd2	7.01	7.02
SWI/SNF related matrix associated actin dependent regulator of chromatin subfamily c member 2	7.01	7.02
MICAL-like 2	7.00	7.00
MGC131041	6.88	7.14
Rho GTPase activating protein 1	6.81	6.97
Vasp	6.81	6.90
Cofilin 1B	6.8	7.30
Smarcd1	6.76	6.64
Actin-related protein 2/3 complex subunit 1b	6.75	6.91
actin related protein 2/3 complex. subunit 1B	6.75	6.91
SWI/SNF-related matrix-associated actin-dependent regulator of chromatin subfamily A-like protein 1	6.67	6.45
WASP	6.55	6.69
Actin-binding LIM protein 2	6.37	6.65
WD repeat-containing protein 1-A	5.92	6.55
actin related protein 2/3 complex. subunit 3	5.85	5.60
Rho GTPase activating protein 21	5.81	5.64
Profilin	5.50	5.72
TRIO and F-actin binding protein	5.35	5.51
Rho GTPase activating protein 5	5.16	5.15
WD repeat-containing protein 1-B	5.01	5.56
Rho-associated kinase alpha	4.91	5.39
Rho GDP-dissociation inhibitor 2	4.88	6.03
ARP8 actin-related protein 8 homolog	4.85	5.14
Afadin- and alpha-actinin-binding protein	4.83	5.24
SWI/SNF-related matrix-associated actin-dependent regulator of chromatin subfamily E member 1-related	4.81	4.94
Actin-related protein 10 homolog	4.72	4.97
Coronin 2B	4.70	5.19
Rho GTPase activating protein 35	4.68	4.75
Anillin	4.40	5.16
Rho GTPase activating proteins 18	0	4.73

CNN3	0	5.25

Table S4: List of formins in the structure proteome of nuclei in our dataset (*X. tropicalis* database)

Gene names	Fasta headers	No of peptides	
		Ctl	CDK-inh
diaph1	F6UXX7_XENTR Uncharacterized protein OS=Xenopus tropicalis	4	4
diaph3	F6VAH9_XENTR Uncharacterized protein (Fragment) OS=Xenopus tropicalis	3	3
fmn2	F6UL32_XENTR Uncharacterized protein OS=Xenopus tropicalis	2	3

Movie 1 Visualization of early G1 nuclear actin filaments in live human cancer cells.

Timelapse confocal microscopy of U2OS cells stably expressing actin-NLS chromobody (green) and transiently transfected with PCNA chromobody (red). Numbers denote time in hr:min; bar, 5µm.

Movie 2 Prolonged expression of Lifeact-GFP-NLS stabilises nuclear actin filaments and impairs cell cycle progression.

Timelapse confocal microscopy of U2OS cells transiently expressing Lifeact-GFP-NLS. Numbers denote time in hr:min; bar, 5µm.

Movie 3 Expression of mDiaDAD.LG in the nucleus impairs replication foci formation.

Timelapse confocal microscopy of S-phase U2OS cells stably expressing the PCNA chromobody (red) and transiently transfected with the mDiaDAD.LG.NLS construct (green). Numbers denote time in hr:min; bar, 5µm.

Movie 4 SMIFH2 impairs nuclear actin dynamics.

Timelapse confocal microscopy of U2OS cells stably expressing actin-NLS chromobody (green), in the presence of SMIFH2 (50 µM). Numbers denote time in hr:min; bar, 5µm.

Movie 5 SMIFH2 stabilises early G1 nuclear actin filaments.

Timelapse confocal microscopy of early G1 U2OS cells stably expressing actin-NLS chromobody (green), in the presence of SMIFH2 (50 µM). Numbers denote time in hr:min; bar, 5µm.

Movie 6 Perturbing nuclear actin dynamics abolishes replication foci formation.

Timelapse confocal microscopy of S-phase U2OS cells stably expressing actin-NLS chromobody (green) transiently transfected with the PCNA chromobody (red), in the presence of SMIFH2 (50 µM). Numbers denote time in hr:min; bar, 5µm

Figure 1

A

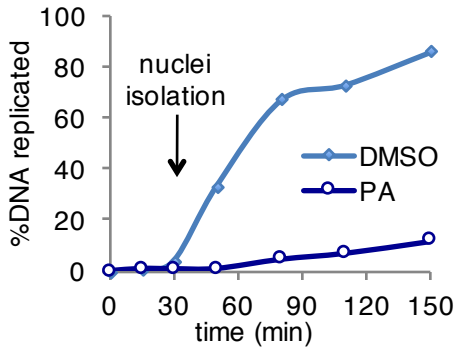

B

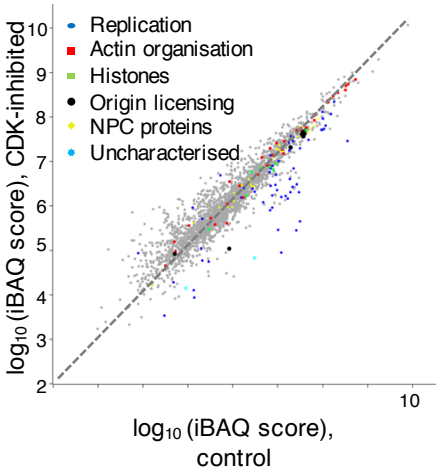

C

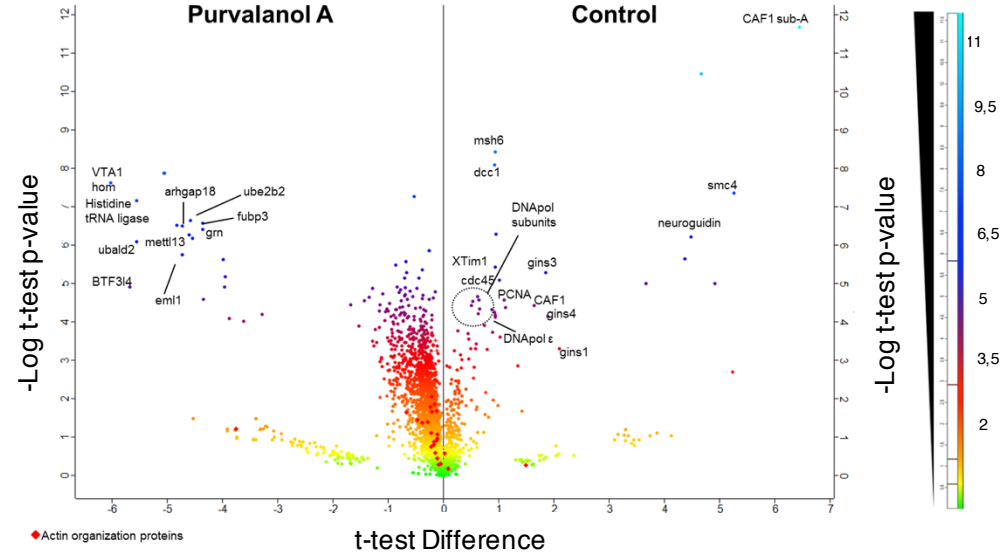

D

GO BP Category	Log10 P-value		
	Entire dataset	Ctrl enriched	CDK1/2-inh. enriched
GO:0006260 I DNA replication	-12.7	-24.1	NE
GO: 0006259 I DNA metabolic process	-21.3	-22.7	NE
GO: 0006297 I DNA gap filling	NE	-10.2	NE
GO:0007049 I Cell cycle	-5.2	-5.4	NE
GO:0000731 I DNA synthesis during DNA repair	NE	-4.0	NE
GO:0006413 I Translation initiation	-4.3	NE	-3.3
GO:0016071 I mRNA metabolic process	-3.6	NE	-2.4
GO:0022402 I Cell cycle process	-2.7	NE	-2.0
GO:0010608 I Posttranscriptional regulation of gene expression	NE	NE	-2.4
GO:0051276 I Chromosome organization	-9.6	NE	NE
GO:0032970 I Regulation of actin filament-based process	-5.9	NE	NE

E

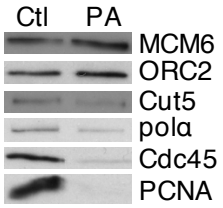

Figure 2

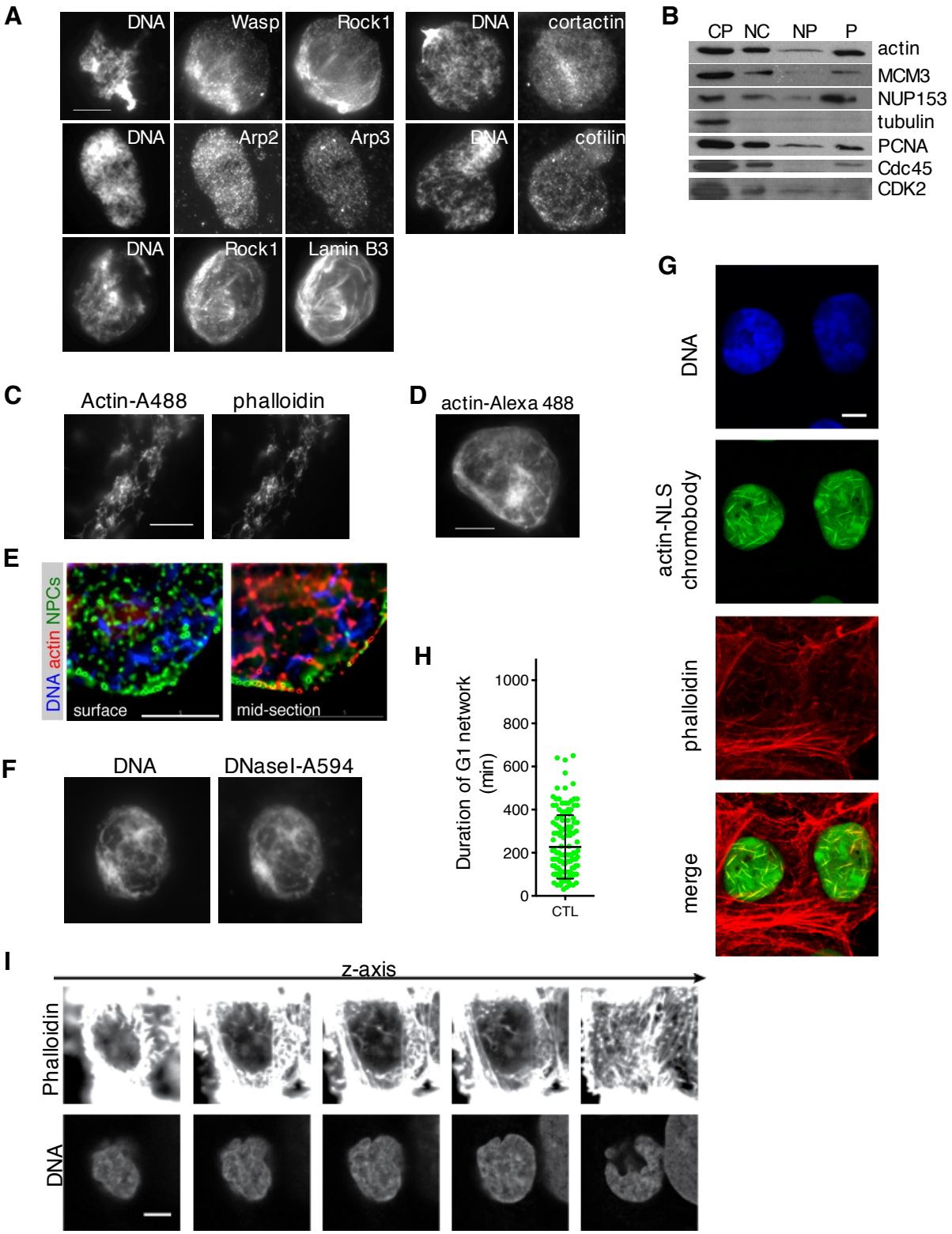
A
DNA
Wasp
Rock1
DNA
cortactin
DNA
Arp2
Arp3
DNA
cofilin
DNA
Rock1
Lamin B3
B
CP NC NP P
actin
MCM3
NUP153
tubulin
PCNA
Cdc45
CDK2
C
Actin-A488
phalloidin
D
actin-Alexa 488
E
DNA actin NPCs
surface
mid-section
F
DNA
DNaseI-A594
G
DNA
actin-NLS chromobody
phalloidin
merge
H
Duration of G1 network (min)
1000
800
600
400
200
0
CTL
I
z-axis
Phalloidin
DNA

Figure 3

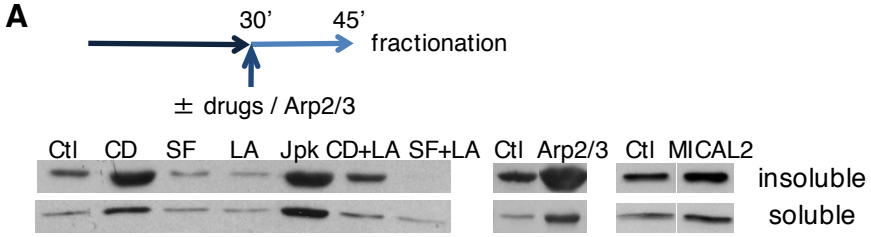
A
30'
45'
fractionation
± drugs / Arp2/3
Ctl CD SF LA Jpk CD+LA SF+LA Ctl Arp2/3 Ctl MICAL2
insoluble
soluble

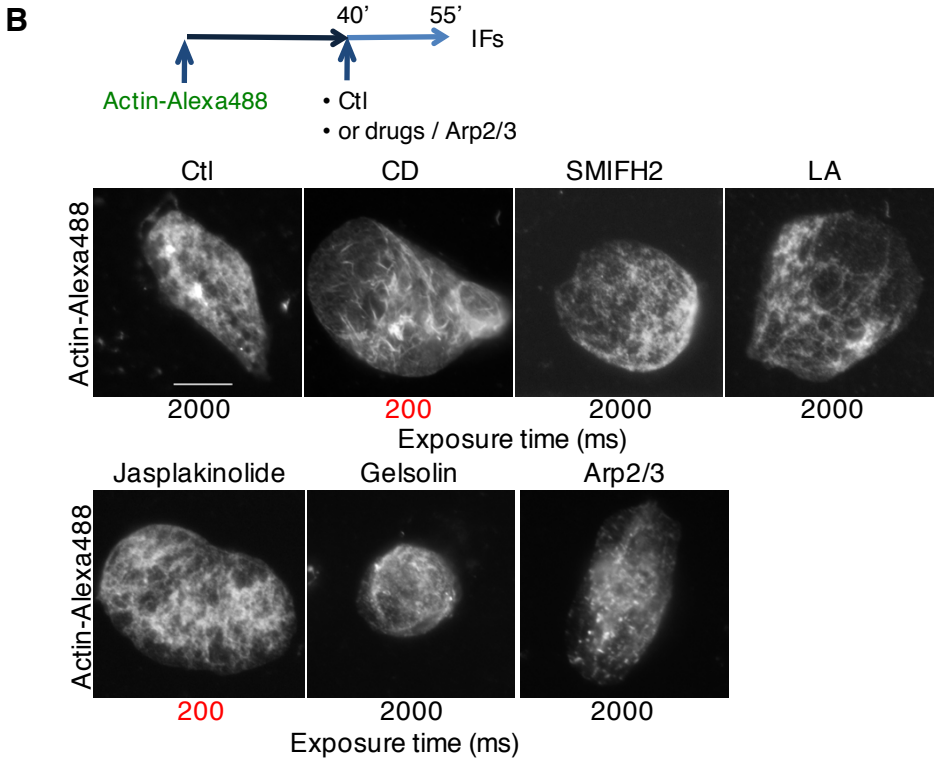
B
40'
55'
IFs
Actin-Alexa488
• Ctl
• or drugs / Arp2/3
Ctl
CD
SMIFH2
LA
Actin-Alexa488
2000
200
2000
2000
Exposure time (ms)
Jasplakinolide
Gelsolin
Arp2/3
Actin-Alexa488
200
2000
2000
Exposure time (ms)

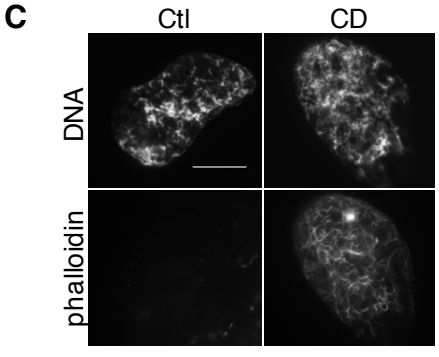
C
Ctl
CD
DNA
phalloidin

Figure 4

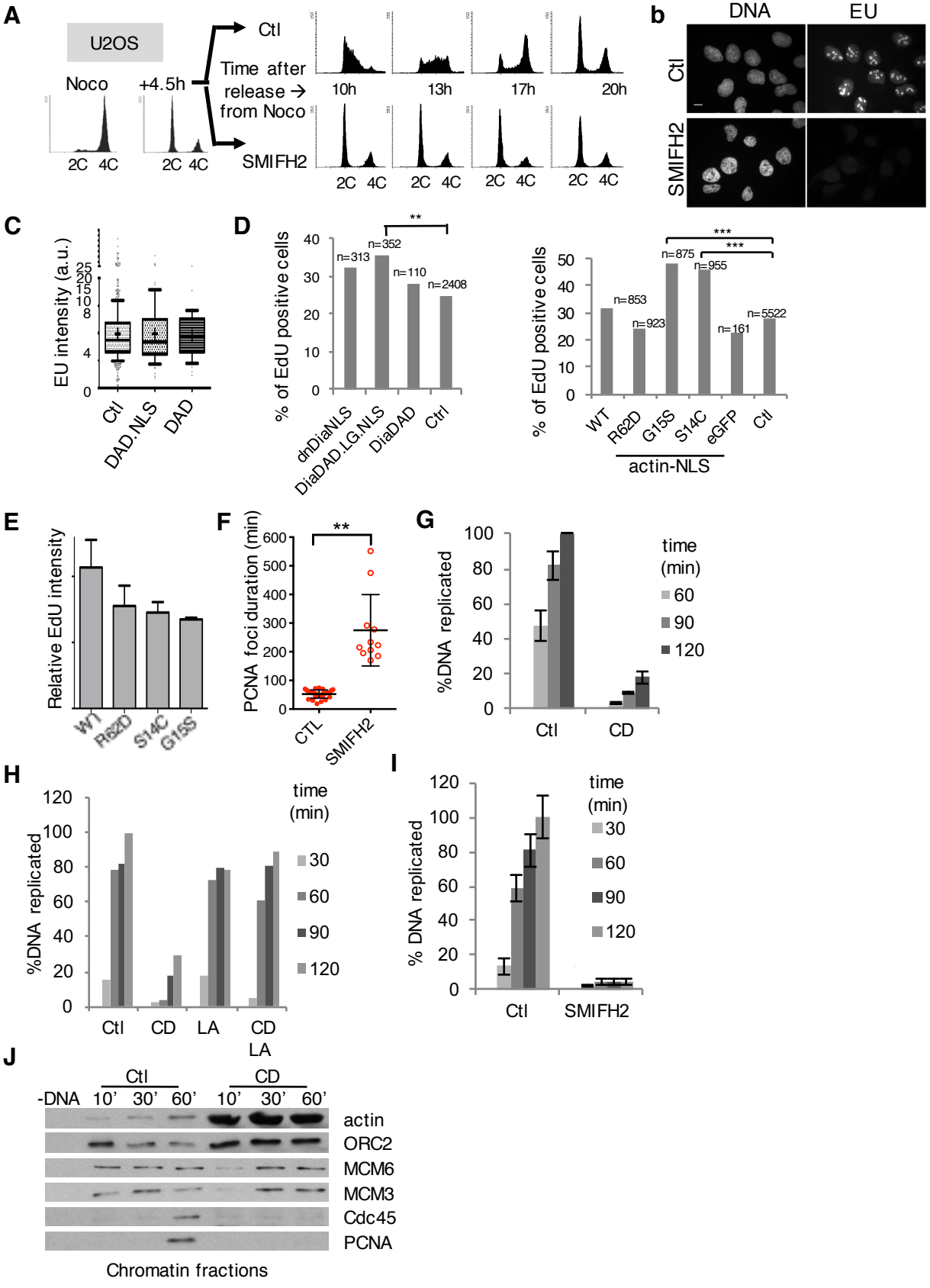
A
U2OS
Noco
+4.5h
Ctl
Time after release → from Noco
SMIFH2
10h
13h
17h
20h
2C 4C
b
DNA
EU
Ctl
SMIFH2
C
EU intensity (a.u.)
Ctl
DAD.NLS
DAD
D
% of EdU positive cells
n=313
n=352
n=110
n=2408
**
dnDiaNLS
DiaDAD.LG.NLS
DiaDAD
Ctrl
n=853
n=923
n=875
n=955
n=161
n=5522
***
WT
R62D
G15S
S14C
eGFP
Ctl
actin-NLS
E
Relative EdU intensity
WT
R62D
S14C
G15S
F
PCNA foci duration (min)
CTL
SMIFH2
G
%DNA replicated
time (min)
60
90
120
Ctl
CD
H
%DNA replicated
time (min)
30
60
90
120
Ctl
CD
LA
CD LA
I
% DNA replicated
time (min)
30
60
90
120
Ctl
SMIFH2
J
Ctl
CD
-DNA
10’
30’
60’
actin
ORC2
MCM6
MCM3
Cdc45
PCNA
Chromatin fractions

Figure 5

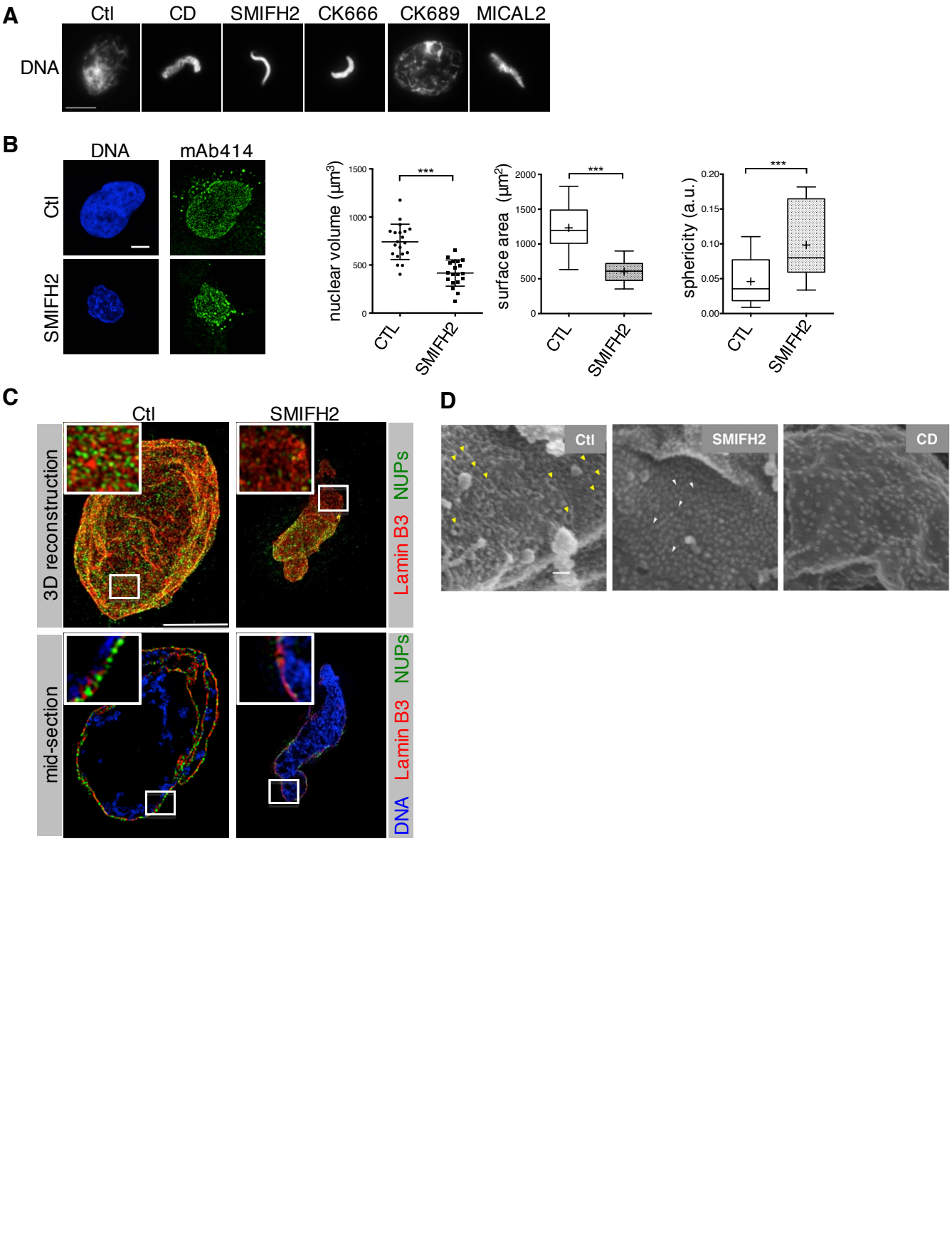
A
Ctl
CD
SMIFH2
CK666
CK689
MICAL2
DNA
B
DNA
mAb414
Ctl
SMIFH2
nuclear volume (µm3)
surface area (µm2)
sphericity (a.u.)
***
CTL
SMIFH2
C
Ctl
SMIFH2
3D reconstruction
mid-section
NUPs
Lamin B3
DNA
D
Ctl
SMIFH2
CD

Figure 6

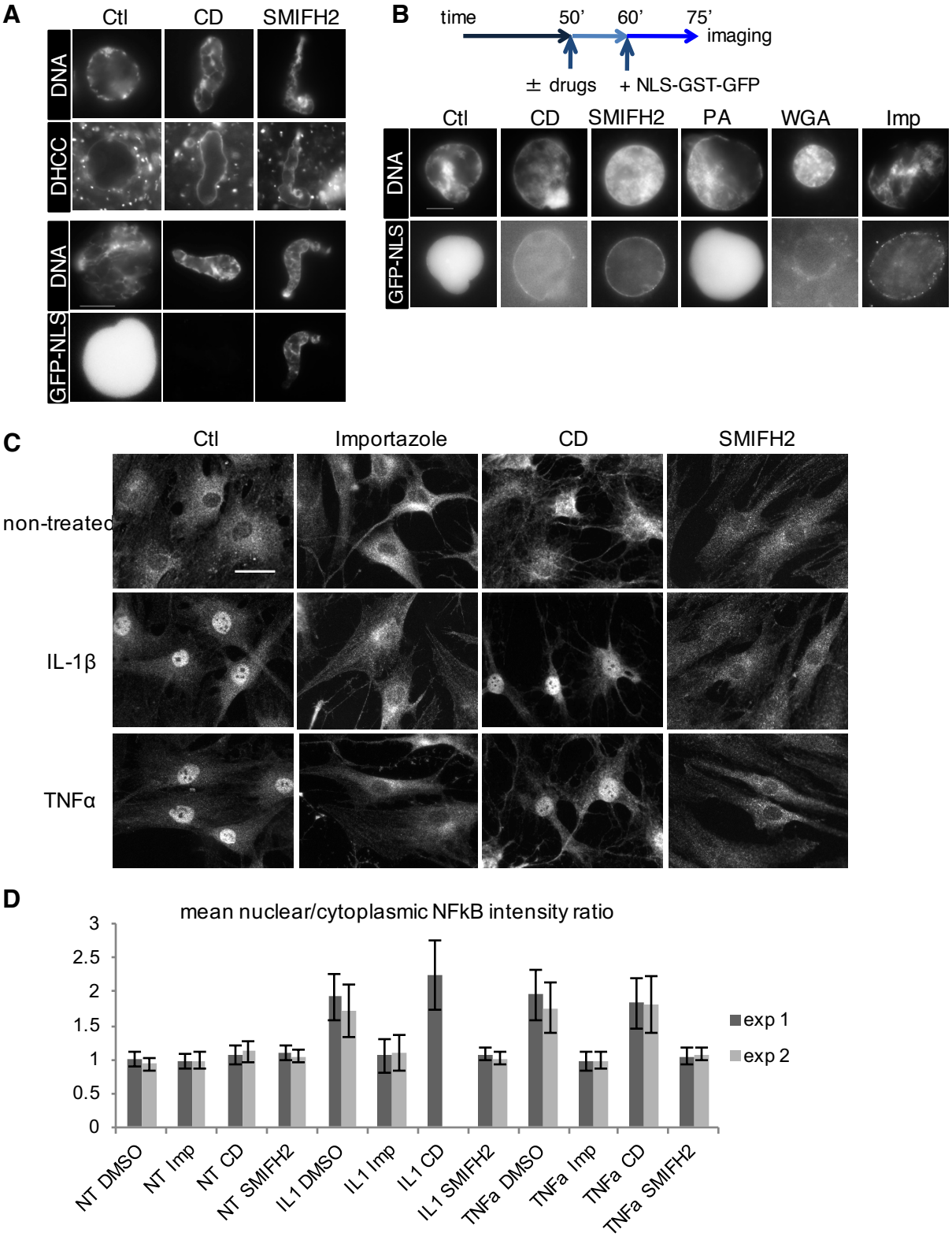
A
Ctl
CD
SMIFH2
DNA
DHCC
DNA
GFP-NLS
B
time
50'
60'
75'
imaging
± drugs
+ NLS-GST-GFP
Ctl
CD
SMIFH2
PA
WGA
Imp
DNA
GFP-NLS
C
Ctl
Importazole
CD
SMIFH2
non-treated
IL-1β
TNFα
D
mean nuclear/cytoplasmic NFkB intensity ratio
3
2.5
2
1.5
1
0.5
0
exp 1
exp 2
NT DMSO
NT Imp
NT CD
NT SMIFH2
IL1 DMSO
IL1 Imp
IL1 CD
IL1 SMIFH2
TNFa DMSO
TNFa Imp
TNFa CD
TNFa SMIFH2

Figure 7

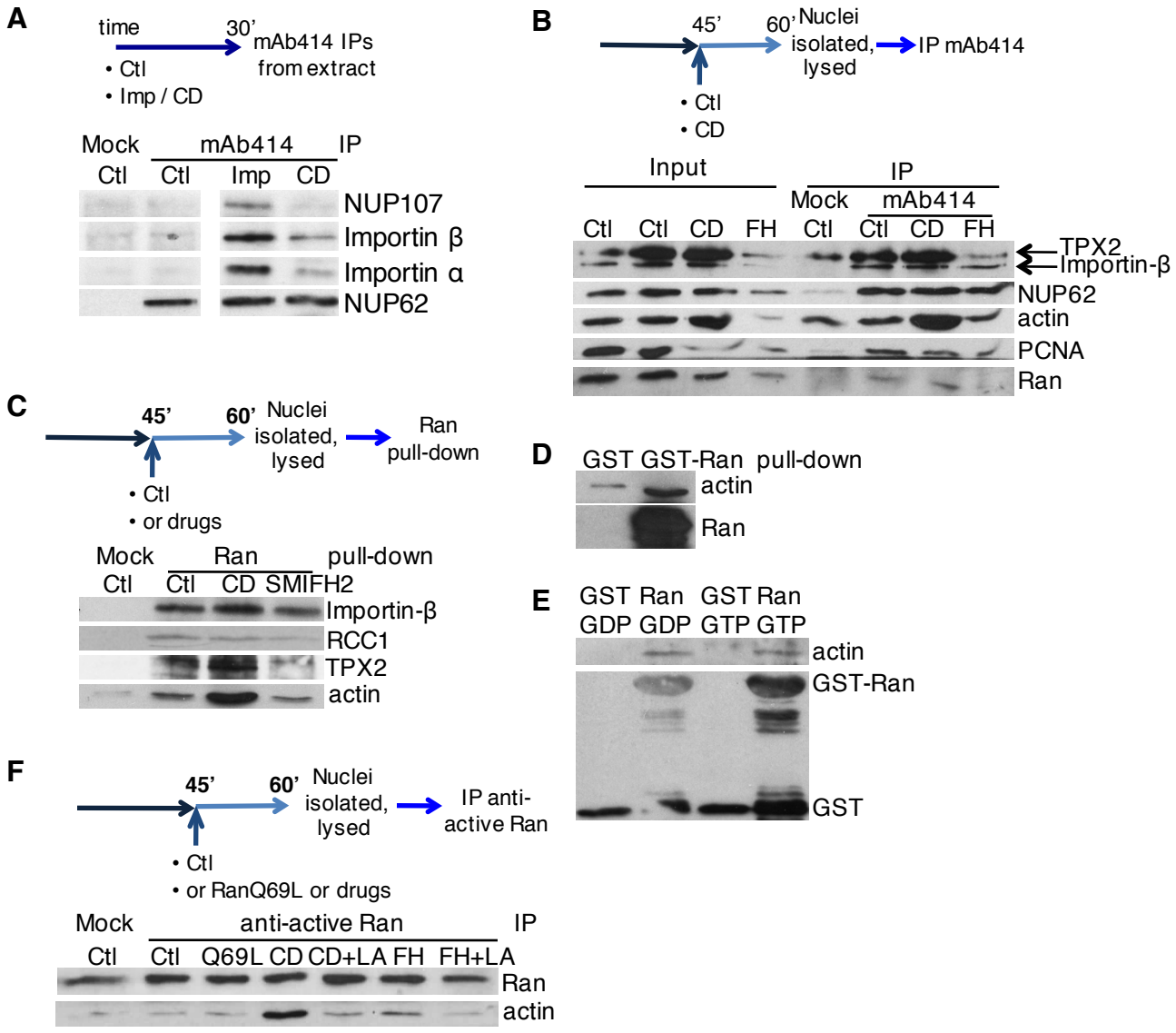
A
time
30'
mAb414 IPs from extract
• Ctl
• Imp / CD
Mock
mAb414
IP
Ctl
Ctl
Imp
CD
NUP107
Importin β
Importin α
NUP62
B
45'
60'
Nuclei isolated, lysed
IP mAb414
• Ctl
• CD
Input
IP
Mock
mAb414
Ctl
Ctl
CD
FH
Ctl
Ctl
CD
FH
TPX2
Importin-β
NUP62
actin
PCNA
Ran
C
45'
60'
Nuclei isolated, lysed
Ran pull-down
• Ctl
• or drugs
Mock
Ran
pull-down
Ctl
Ctl
CD
SMIFH2
Importin-β
RCC1
TPX2
actin
D
GST
GST-Ran
pull-down
actin
Ran
E
GST
Ran
GST
Ran
GDP
GDP
GTP
GTP
actin
GST-Ran
GST
F
45'
60'
Nuclei isolated, lysed
IP anti-active Ran
• Ctl
• or RanQ69L or drugs
Mock
anti-active Ran
IP
Ctl
Ctl
Q69L
CD
CD+LA
FH
FH+LA
Ran
actin

Figure 8

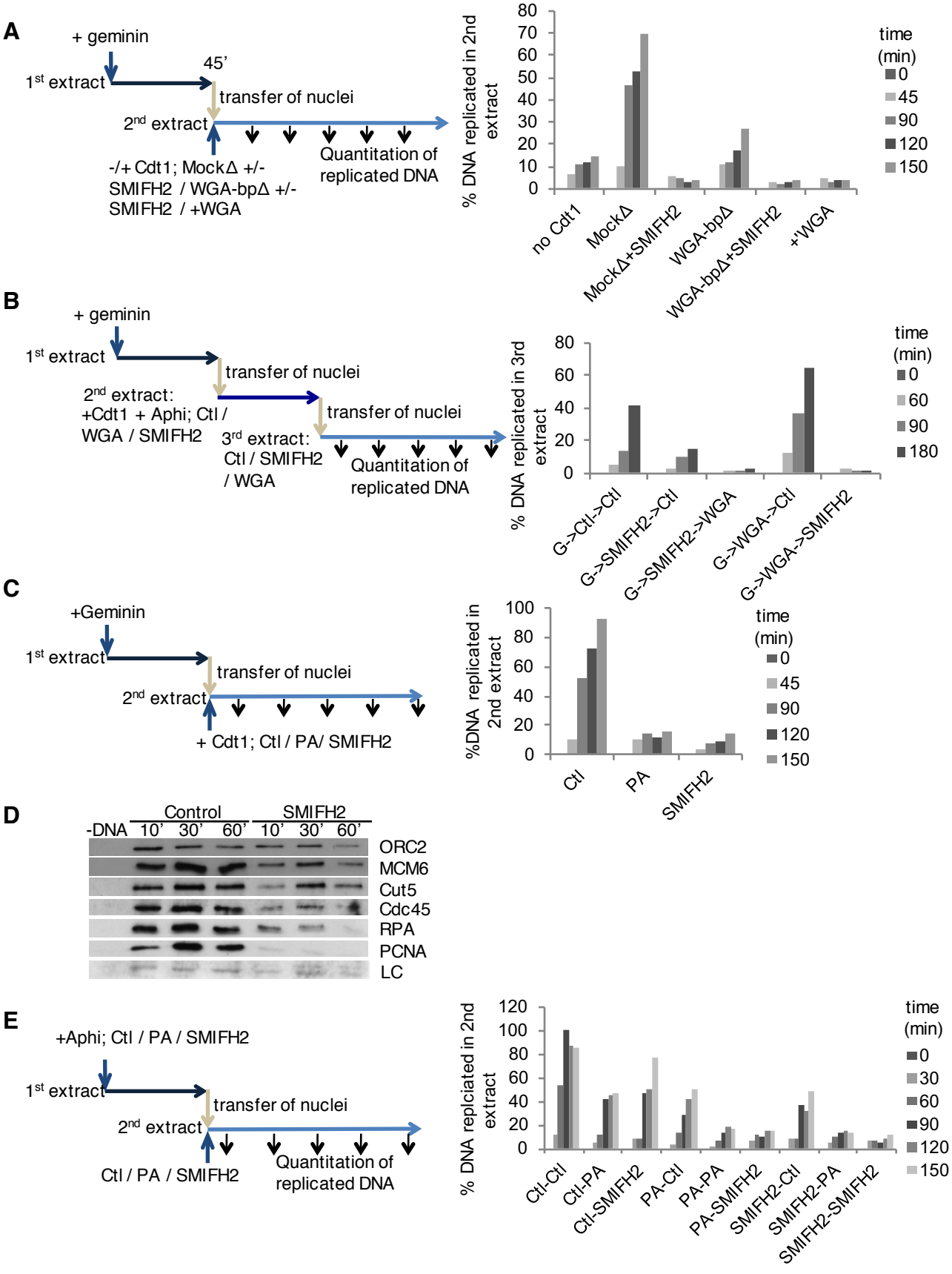
A
+ geminin
1st extract
45'
transfer of nuclei
2nd extract
-/+ Cdt1; MockΔ +/- SMIFH2 / WGA-bpΔ +/- SMIFH2 / +WGA
Quantitation of replicated DNA
% DNA replicated in 2nd extract
time (min)
0
45
90
120
150
no Cdt1
MockΔ
MockΔ+SMIFH2
WGA-bpΔ
WGA-bpΔ+SMIFH2
+WGA
B
+ geminin
1st extract
transfer of nuclei
2nd extract: +Cdt1 + Aphi; Ctl / WGA / SMIFH2
transfer of nuclei
3rd extract: Ctl / SMIFH2 / WGA
Quantitation of replicated DNA
% DNA replicated in 3rd extract
time (min)
0
60
90
180
G->Ctl->Ctl
G->SMIFH2->Ctl
G->SMIFH2->WGA
G->WGA->Ctl
G->WGA->SMIFH2
C
+Geminin
1st extract
transfer of nuclei
2nd extract
+ Cdt1; Ctl / PA/ SMIFH2
%DNA replicated in 2nd extract
time (min)
0
45
90
120
150
Ctl
PA
SMIFH2
D
Control
SMIFH2
-DNA
10'
30'
60'
10'
30'
60'
ORC2
MCM6
Cut5
Cdc45
RPA
PCNA
LC
E
+Aphi; Ctl / PA / SMIFH2
1st extract
transfer of nuclei
2nd extract
Ctl / PA / SMIFH2
Quantitation of replicated DNA
% DNA replciated in 2nd extract
time (min)
0
30
60
90
120
150
Ctl-Ctl
Ctl-PA
Ctl-SMIFH2
PA-Ctl
PA-PA
PA-SMIFH2
SMIFH2-Ctl
SMIFH2-PA
SMIFH2-SMIFH2

Figure 9

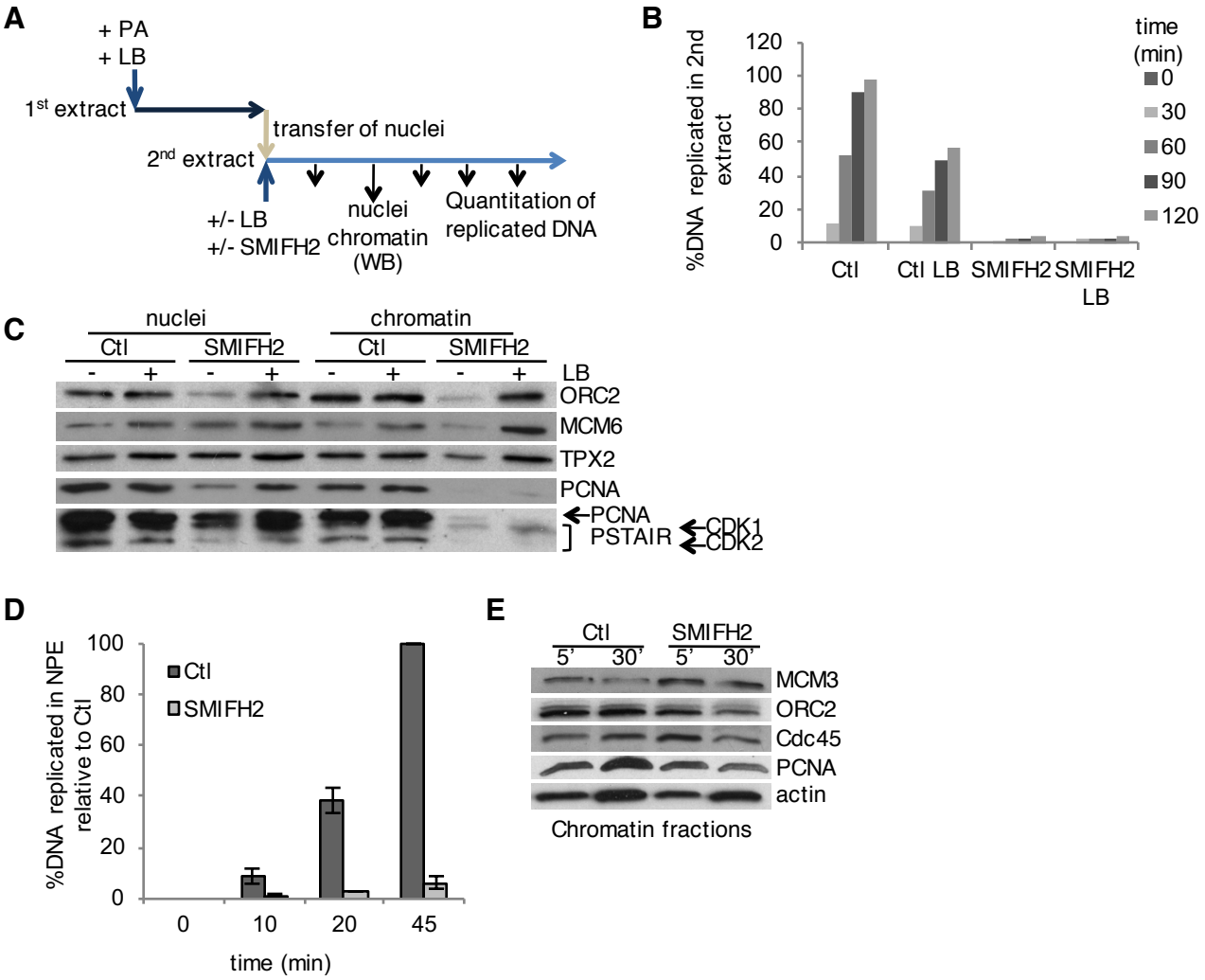
A
+ PA
+ LB
1st extract
transfer of nuclei
2nd extract
+/- LB
+/- SMIFH2
nuclei
chromatin
(WB)
Quantitation of
replicated DNA
B
%DNA replicated in 2nd extract
120
100
80
60
40
20
0
time (min)
0
30
60
90
120
Ctl
Ctl LB
SMIFH2
SMIFH2 LB
C
nuclei
chromatin
Ctl
SMIFH2
Ctl
SMIFH2
- + - + - + - +
LB
ORC2
MCM6
TPX2
PCNA
PCNA
PSTAIR
CDK1
CDK2
D
%DNA replicated in NPE relative to Ctl
100
80
60
40
20
0
Ctl
SMIFH2
0
10
20
45
time (min)
E
Ctl
SMIFH2
5’ 30’ 5’ 30’
MCM3
ORC2
Cdc45
PCNA
actin
Chromatin fractions

Supplementary Figure 1

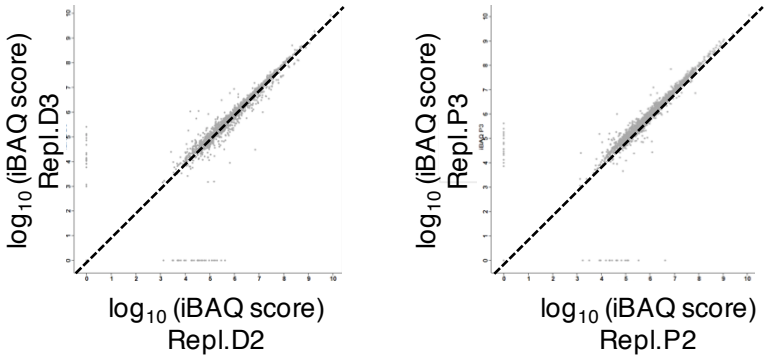

Supplementary Figure 2

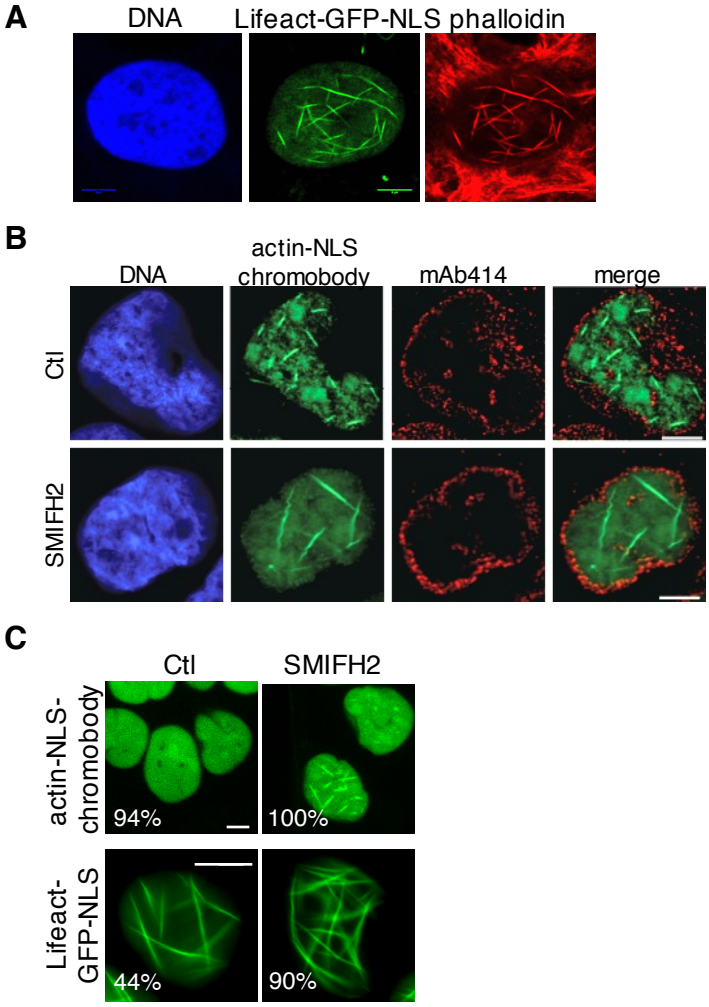

Supplementary Figure 3

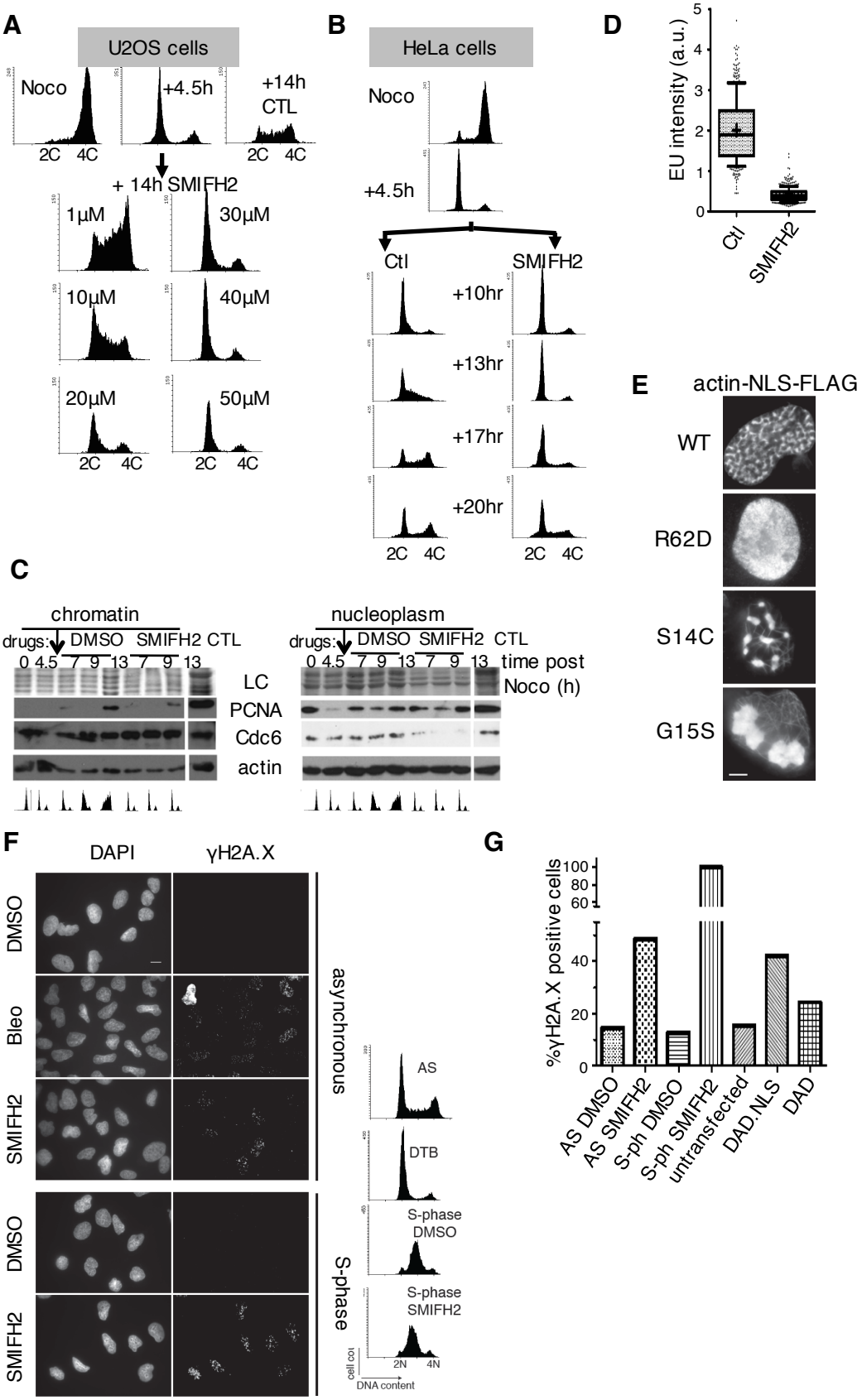

Supplementary Figure 4

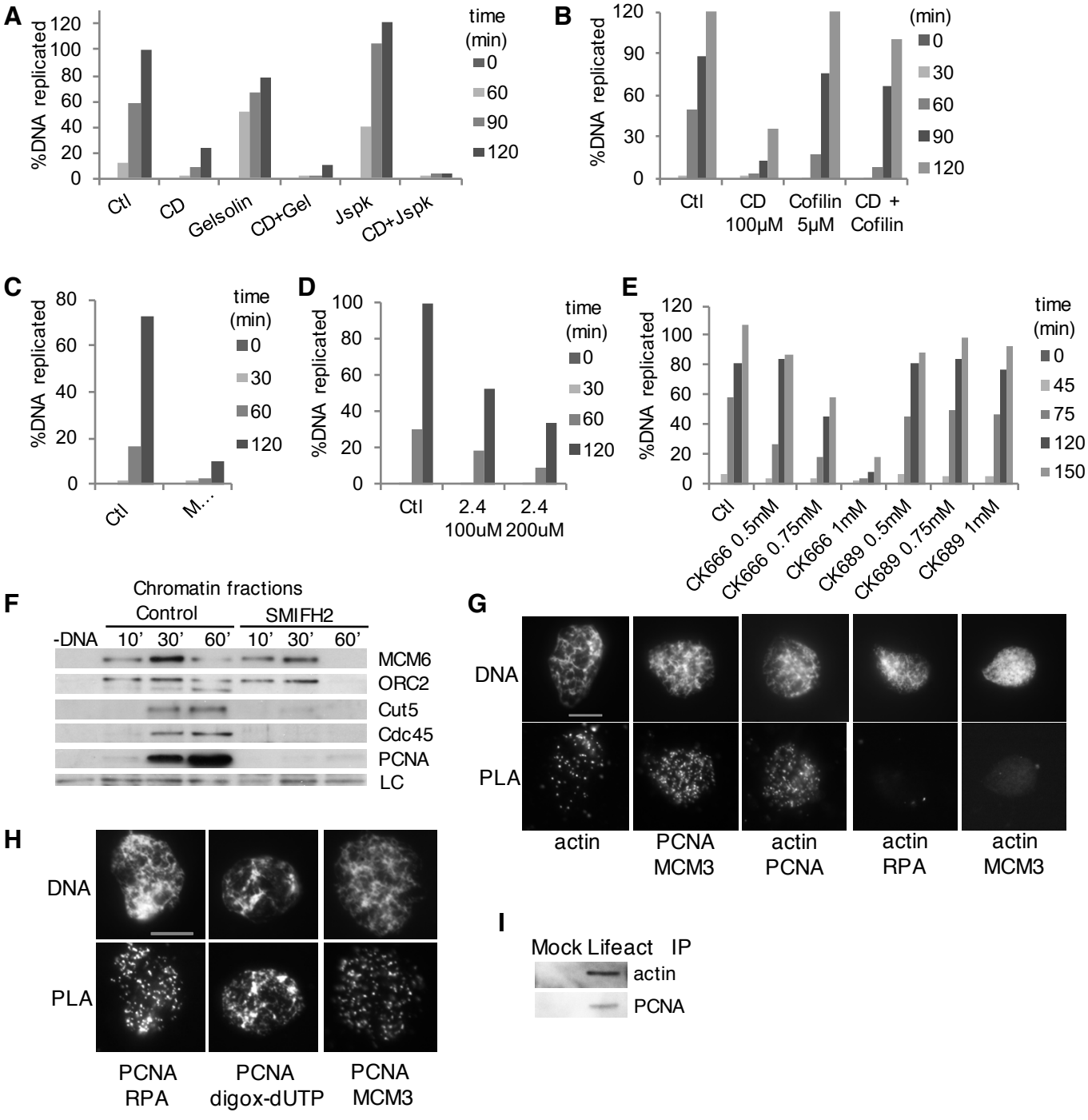

Supplementary Figure 5

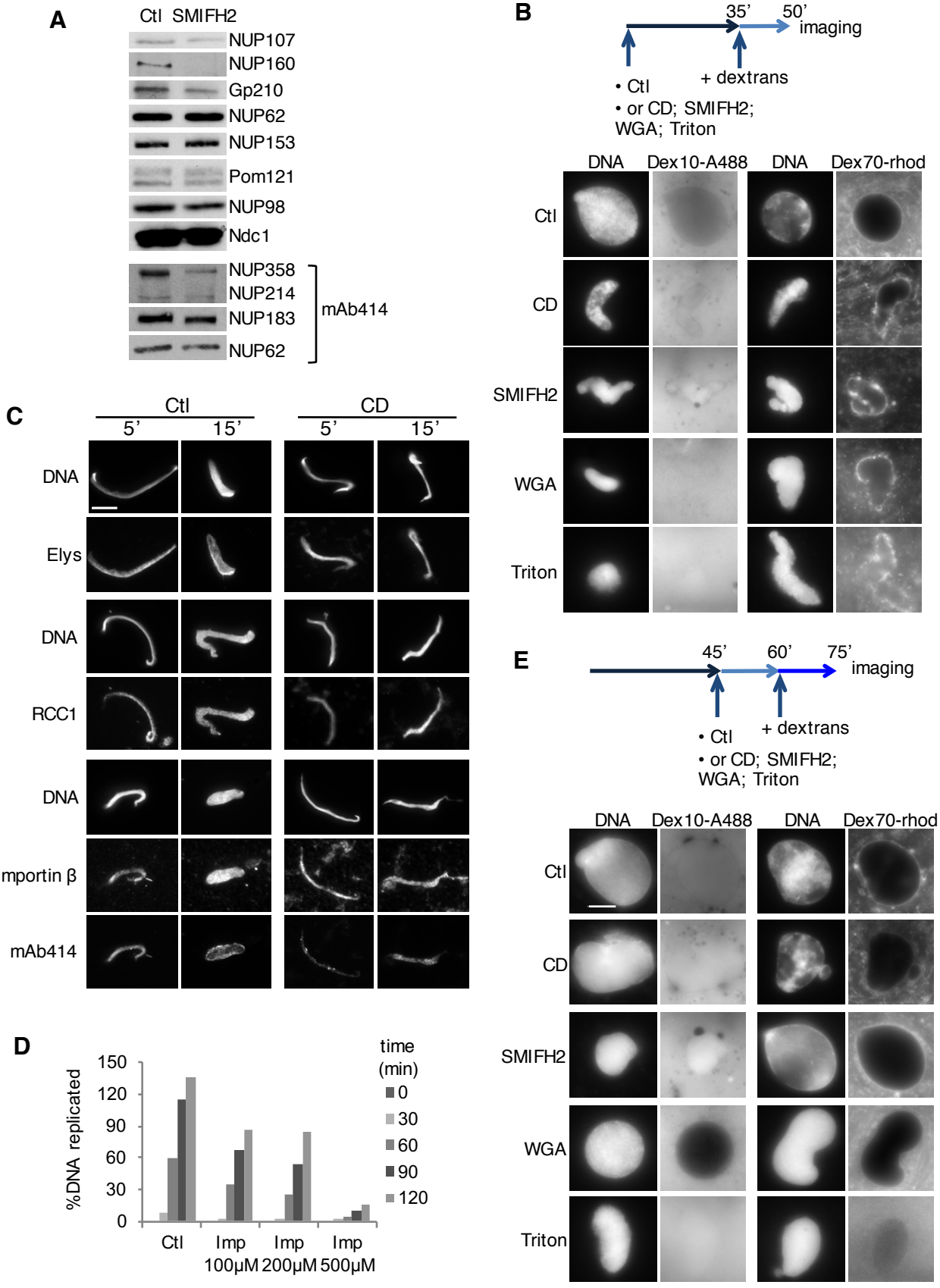

Supplementary Figure 6